

Journal Pre-proof

Synthesis, photophysical characterization, CASSCF/CASPT2 calculations and CT-DNA interaction study of amino and azido benzazole analogues

Eduarda S. Gil, Cláudia B. da Silva, Pablo A. Nogara, Carolina H. da Silveira, João B.T. da Rocha, Bernardo A. Iglesias, Diogo S. Lüdtkke, Paulo F.B. Gonçalves, Fabiano S. Rodembusch

PII: S0167-7322(19)34500-3

DOI: <https://doi.org/10.1016/j.molliq.2019.111938>

Reference: MOLLIQ 111938

To appear in: *Journal of Molecular Liquids*

Received Date: 9 August 2019

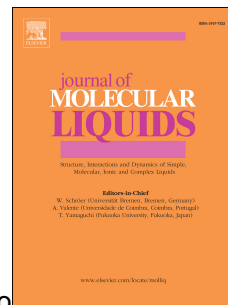
Revised Date: 26 September 2019

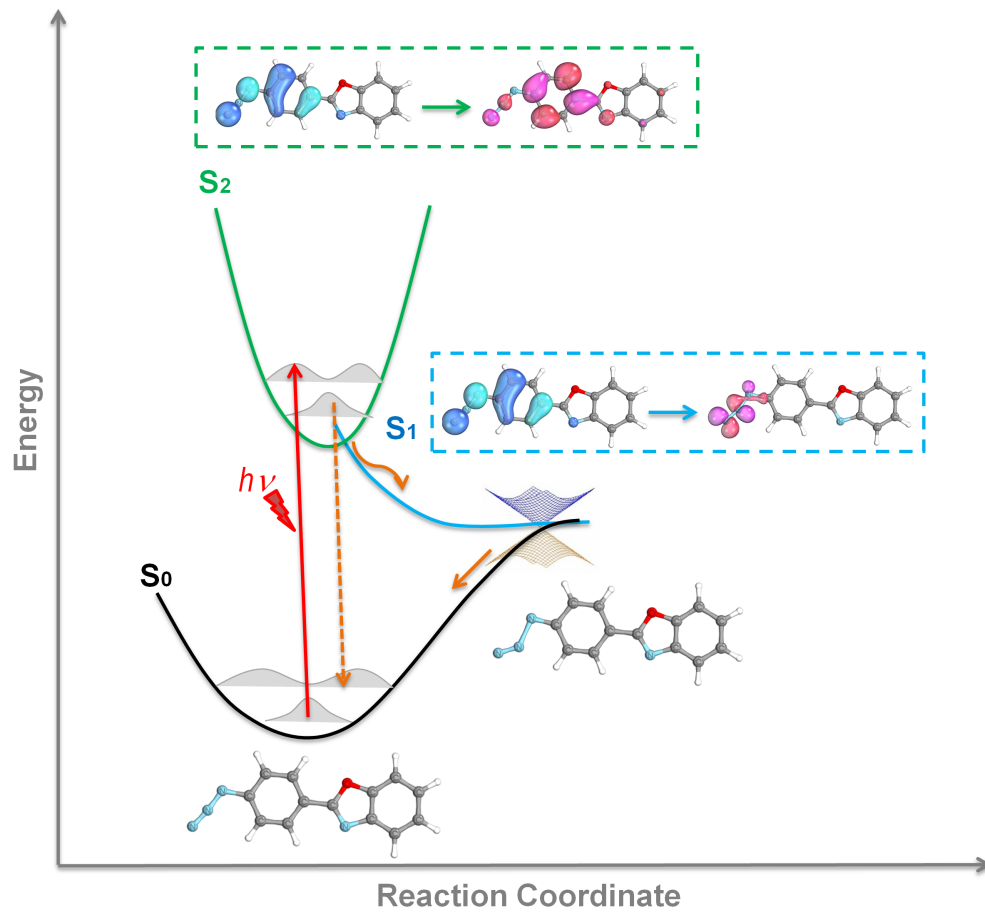
Accepted Date: 14 October 2019

Please cite this article as: E.S. Gil, Clá.B. da Silva, P.A. Nogara, C.H. da Silveira, João B.T. da Rocha, B.A. Iglesias, D.S. Lüdtkke, P.F.B. Gonçalves, F.S. Rodembusch, Synthesis, photophysical characterization, CASSCF/CASPT2 calculations and CT-DNA interaction study of amino and azido benzazole analogues, *Journal of Molecular Liquids* (2019), doi: <https://doi.org/10.1016/j.molliq.2019.111938>.

This is a PDF file of an article that has undergone enhancements after acceptance, such as the addition of a cover page and metadata, and formatting for readability, but it is not yet the definitive version of record. This version will undergo additional copyediting, typesetting and review before it is published in its final form, but we are providing this version to give early visibility of the article. Please note that, during the production process, errors may be discovered which could affect the content, and all legal disclaimers that apply to the journal pertain.

© 2019 Published by Elsevier B.V.





Synthesis, photophysical characterization, CASSCF/CASPT2 calculations and CT-DNA interaction study of amino and azido benzazole analogues

Eduarda S. Gil,^{at} Cláudia B. da Silva,^{at} Pablo A. Nogara,^b Carolina H. da Silveira,^c João B. T. da Rocha,^b Bernardo A. Iglesias,^c Diogo S. Lüdtkke,^a Paulo F. B. Gonçalves,^{*a} Fabiano S. Rodembusch^{*a}

^aInstituto de Química, Universidade Federal do Rio Grande do Sul, UFRGS. Av. Bento Gonçalves 9500, 91501-970, Porto Alegre, RS, Brazil. E-mail: rodembusch@iq.ufrgs.br (Fabiano S. Rodembusch) and paulo@iq.ufrgs.br (Paulo F. B. Gonçalves)

^bLaboratório de Bioquímica Toxicológica, Departamento de Bioquímica e Biologia Molecular, Universidade Federal de Santa Maria, 97105-900, Santa Maria, RS, Brazil.

^cLaboratório de Bioinorgânica e Materiais Porfirínicos, Universidade Federal de Santa Maria, 97105-900, Santa Maria, RS, Brazil.

[†]Both authors contributed equally to this work

Abstract

This work describes the synthesis and photophysical investigation of amino and azido benzazoles. The amino derivatives were obtained by condensation reaction between ortho-substituted anilines and p-aminobenzoic in polyphosphoric acid. The respective azides were synthesized by reaction of diazonium salts from the previously prepared amines with sodium azide. These compounds present absorption maxima in the UV-A region, nm ascribed to fully spin and symmetry electronic transitions. All compounds presented a main fluorescence emission in the UV-A to the violet region with a relatively large Stokes shift. The latter related to a solvent dependence. The amino derivatives presented higher values to the fluorescence quantum yields in despite of the azido analogues. DFT, TD-DFT and multiconfigurational calculations (SA-CASSCF and MS-CASPT2) were performed in order to investigate the photophysical features of these molecules, mainly on the azide derivatives, where the main interest was the investigation of the intrinsic fluorescence

quenching present in these compounds. In this sense, it was observed that the weak fluorescence emission observed in the azide compounds could be related to the dissociative character of the S_1 state, which reaches a conical intersection point between S_1/S_0 states, and through this point, goes back to the ground state by a nonradioactive decay. In addition, the DNA binding assays by UV-Vis absorption and fluorescence emission methodologies indicated that the benzazoles presented strong interaction with CT-DNA, which could be attributed to π -stacking and/or intermolecular hydrogen-bonding. Docking was also performed to better understand the observed interaction.

1. Introduction

Benzazoles are a class of heterocyclic compounds with numerous applications in pharmaceuticals and materials science [1]. These scaffolds consist of the fusion of benzene and the azole moiety [2]; this latter constituted by five atoms of which two are heteroatoms in positions 1 and 3, and one of them always being the nitrogen atom [3]. These compounds can exhibit interesting photophysical properties, such as fluorescence emission with large Stokes shift and high photostability [4-9]. In this regard, several methods of preparing benzazoles are described in the literature, including for instance intramolecular cyclization, catalyzed cyclization of o-haloanilides and condensation of o-substituted anilines with carboxylic acids, acyl esters and chlorides, amides, nitriles or even aromatic aldehydes [10-19]. Among this class of compounds, several benzazole derivatives have been described with inhibitory activity in various enzymatic reactions allowing its investigation to treat or even prevent diseases [20-23]. In this context, several benzothiazole derivatives have also shown antibacterial, anticancer, anti-oxidant, antiviral, anti-tuberculosis, anti-diabetic and anti-inflammatory activities [24-29]. In addition, the particular photophysical properties, as well as their planar structures, make them suitable for use as fluorescent probes to study biological mechanisms in protein and DNA [30-35]. In this context, another class of molecules able to act as DNA probes are the azide based compounds, through the DNA hybridization. In this approach, a single-stranded DNA probe (ssDNA) is immobilized on a surface and exposed to a sample containing the

complementary target sequence characteristics, which is captured by the formation of a double-stranded DNA (dsDNA). This event, so-called hybridization, is then translated into a signal. A variety of transduction techniques can be used to observe this process, including the optical one [36,37].

Thus, the present study presents the synthesis of benzazole heterocycles containing amino and azido groups, as well as their photophysical study and the application to study the interaction with CT-DNA. The photophysical characterization and the interaction study were complemented with theoretical calculations and docking, respectively.

2. Experimental

2.1. Materials and methods

All reagents were used as received and the solvents were purchased from commercial sources and purified according to the literature [38]. The reactions were monitored by Thin Layer Chromatography (TLC) using Silica Gel 60 F254. Fourier transform infrared (FTIR) spectra in the range 600-4000 cm^{-1} and in KBr pellets were recorded on a Varian model 640-IR with a resolution of 4 cm^{-1} . Hydrogen and carbon nuclear magnetic resonance spectra in CDCl_3 (^1H and ^{13}C NMR) were recorded in CDCl_3 at 400 and 100 MHz, respectively. The chemical shifts (δ) are reported in parts per million (ppm) relative to TMS (0.00 ppm), and the coupling constants J are reported in hertz (Hz). Melting points were obtained on a QUIMIS model Q340S and are uncorrected. In the photophysical studies, spectroscopic-grade solvents were used. ESI-QTOF-MS measurements were performed in the positive ion mode (m/z 50-2000 range). The UV-Vis spectra were recorded on a Shimadzu UV-2450 spectrophotometer, and the steady-state fluorescence spectra were measured on a Shimadzu spectrofluorometer model RF-5301PC. The quantum yields of fluorescence (Φ_{FL}) were measured at 25°C using solutions with absorbance intensity lower than 0.05 (optical dilute regime). In these experiments the emission spectra were obtained using slits of 1.5 nm/1.5 nm (Exc/Em). Quinine sulfate in H_2SO_4 1N was used as the quantum yield standards [39].

2.2. Synthesis

General procedure for the synthesis of amino benzoxazoles 4-5

An equimolar mixture of o-aminophenol (**1**) (2.4 g, 22.0 mmol) or o-aminothiophenol (**2**) (2.7 mL, 22.0 mmol) and p-aminobenzoic acid (**3**) (3.0 g, 22.0 mmol) in polyphosphoric acid (20 mL) was stirred at 170°C for 5 h. After cooling, the mixture was poured onto ice under vigorous stirring. The solution was neutralized with NaHCO₃. The precipitate was filtered, washed with water and dried at 60°C. The solid was purified by column chromatography using dichloromethane as eluent [40].

2-(4'-Amino)benzoxazole (**4**) [41]. Yield: 69% (1.7 g). Melting point: 150-152°C. FTIR (KBr, cm⁻¹): 3497 (ν_{as} N-H), 3325 (ν_s N-H), 3000 (ν_{arom} C-H), 1620 and 1470 (ν_{arom} C=C). ¹H NMR (400 MHz, CDCl₃) δ 8.10-8.04 (m, 2H), 7.76-7.70 (m, 1H), 7.57-7.52 (m, 1H), 7.36-7.28 (m, 2H), 6.79-6.75 (m, 2H), 4.21 (s, 2H). APT (101 MHz, CDCl₃) δ 163.8, 150.5, 149.7, 142.4, 129.4, 124.3, 124.2, 119.9, 116.8, 114.7, 110.2.

2-(4'-Amino)benzothiazole (**5**) [42]. Yield: 63% (1.4 g). Melting point: 161-163°C. FTIR (KBr, cm⁻¹): 3497 (ν_{as} N-H), 3325 (ν_s N-H), 3000 (ν_{arom} C-H), 1620 and 1470 (ν_{arom} C=C). ¹H NMR (400 MHz, CDCl₃) δ 7.87 (dd, *J*=13.9 and 7.9 Hz, 3H), 7.46 (t, *J*=7.6 Hz, 3H), 7.34 (t, *J*=7.6 Hz, 1H), 6.34 (d, *J*=2.0 Hz, 1H), 6.28 (dd, *J*=8.4 and 2.1 Hz, 1H), 4.25 (s, 2H). APT (101 MHz, CDCl₃) δ 169.6, 159.8, 150.9, 131.9, 130.0, 126.4, 121.4, 121.3, 108.5, 107.2, 101.7.

General procedure for the synthesis of azido benzoxazoles 6-7

In a 50 mL round bottom flask under an ice bath containing 2.0 mmol of the benzazole precursors **4-5** (2.0 mmol) and a HCl:H₂O (3:1) solution (15 mL) it was added dropwise a NaNO₂ (0.166 g, 2.4 mmol) solution (1mL). The reaction mixture was stirred under ice bath for 30 min. After this time, NaN₃ was added (0.260 g, 4.0 mmol). The reaction mixture was stirred at room temperature for 2h. After this time, the solution was neutralized with NH₄OH, extracted with ethyl acetate (3x20 mL) and concentrated under reduced pressure to yield the respective product.

2-(4'-Azido)benzoxazole (**6**) [41]. Yield: 71% (0.453 g). Melting point: 128-130°C. FTIR (ATR, cm^{-1}): 3077 ($\nu_{\text{arom C-H}}$), 2077 ($\nu_{\text{-N=N=N}}$), 1513 and 1452 ($\nu_{\text{arom C=C}}$). $^1\text{H NMR}$ (400 MHz, CDCl_3) δ 8.28-8.22 (m, 1H), 7.83-7.74 (m, 1H), 7.62-7.55 (m, 1H), 7.43-7.32 (m, 1H), 7.20-7.12 (m, 1H). APT (75 MHz, CDCl_3) δ 150.8, 143.4, 142.1, 129.2, 125.1, 124.6, 123.8, 119.9, 119.5, 110.5. HRMS (ESI-TOF) m/z : $[\text{M}+\text{H}]^+$ Calcd for $\text{C}_{13}\text{H}_8\text{N}_4\text{O}$ 237.0776; Found 237.0782.

2-(4'-Azido)benzothiazole (**7**). Yield: 78% (0.431 g). Melting point: 154-156°C. FTIR (ATR, cm^{-1}): 3046 ($\nu_{\text{arom C-H}}$), 2108 ($\nu_{\text{-N=N=N}}$), 1602 and 1482 ($\nu_{\text{arom C=C}}$). $^1\text{H NMR}$ (400 MHz, CDCl_3) δ 8.12-8.06 (m, 1H), 7.91 (d, $J=7.6$ Hz, 1H), 7.52-7.49 (m, 1H), 7.44-7.37 (m, 1H), 7.16-7.12 (m, 1H). APT (75 MHz, CDCl_3) δ 167.1, 154.3, 142.8, 135.3, 130.6, 129.0, 126.4, 125.2, 123.1, 121.6, 119.5. HRMS (ESI-TOF) m/z : $[\text{M}+\text{H}]^+$ Calcd for $\text{C}_{13}\text{H}_8\text{N}_4\text{S}$ 253.0548; Found 253.0549.

2.3. CT-DNA binding study

For calf-thymus DNA (CT-DNA) interaction studies with amino and azido derivatives UV-Vis absorption measurements were performed at room temperature in Tris-HCl buffer at pH 7.2, using DMSO stock solution of derivatives (10^{-4} M). The DNA pair base concentrations of low molecular weight CT-DNA were determined using the molar extinction coefficient of 13,200 $\text{M}^{-1}\cdot\text{cm}^{-1}$ (per base pair) at absorption maximum of 260 nm. Compound solutions in DMSO (2%)/Tris-HCl buffer mixture were titrated with increasing concentrations of CT-DNA (ranging from 0-100 μM). Changes in absorption spectra of derivatives were acquired and observed in the wavelength range of 290-500 nm. The intrinsic binding constants (K_b) of derivatives **4-5** and **6-7** were calculated according to the decay of the absorption bands of compounds using the following Equation (1) through a plot of $[\text{DNA}]/(\epsilon_a - \epsilon_f)$ versus $[\text{DNA}]$,

$$[\text{DNA}]/(\epsilon_a - \epsilon_f) = [\text{DNA}]/(\epsilon_b - \epsilon_f) + 1/K_b(\epsilon_b - \epsilon_f) \quad (1)$$

where $[\text{DNA}]$ is the concentration of DNA in the base pairs, ϵ_a is the extinction coefficient ($A_{\text{obs}}/[\text{compound}]$), ϵ_b and ϵ_f are the extinction coefficients of free and

fully bound forms, respectively. In the plots of $[DNA]/(\epsilon_a - \epsilon_f)$ versus $[DNA]$, K_b is given by the slope/interception ratio.

In EB-DNA competitive assays, steady-state emission fluorescence analysis was recorded and the amino and azido derivatives were dissolved in DMSO (10^{-4} M range) and competitive studies were performed through the gradual addition of the stock solution of the derivatives to the quartz cuvette (1.0 cm path length) containing ethidium bromide (EB, 2.0×10^{-7} M) and CT-DNA (2.0×10^{-5} M) in a Tris-HCl pH 7.2 buffer solution. The concentration of derivatives ranged from 0 to 100 μ M. In these studies an excitation wavelength of 510 nm was used and the respective fluorescence emission spectra were recorded in the range of 550-800 nm, 5 min after each addition of the derivative solution in order to allow incubation to occur. The fluorescence quenching Stern-Volmer constants (K_{SV}) of compounds were calculated according to the decay of the emission bands of EB-DNA using the following Equation (2) through a plot of F_0/F versus $[DNA]$,

$$F_0/F = 1 + k_q \tau_0 [Q] = 1 + K_{SV} [Q] \quad (2)$$

where F and F_0 are the fluorescence intensities in the presence and absence of a quencher, respectively [43]. K_{SV} , k_q , τ_0 and $[Q]$ denote Stern-Volmer quenching constant, quenching rate constant, lifetime of EB-DNA adducts (23.0×10^{-9} s) [44] and the concentration of quencher, respectively. According to Equation (2), the Stern-Volmer constants (K_{SV}) were calculated from the slope and k_q is equal K_{SV}/τ_0 . In order to quantify the displacement, the concentration of the heterocycle derivatives at which EB fluorescence decreases by 50% (in this case, assumed to be 50% displacement of EB) is calculated [45]. The values of apparent DNA-binding constant (K_{app}) were calculated using the Equation (3):

$$K_{EB}[EB] = K_{app}[\text{compound}] \quad (3)$$

where K_{EB} ($4.94 \times 10^5 \text{ M}^{-1}$) is the DNA-binding constant of ethidium bromide, $[EB]$ is the concentration of EB (1.50×10^{-6} M), and $[\text{compound}]$ is the concentration of the derivative used to obtain 50% reduction in fluorescence

emission intensity of EB. The standard Gibbs free-energy (ΔG^0) of benzazole-DNA complex was calculated from the values of binding constant (K_b) using the following Equation (4):

$$\Delta G^0 = -RT \ln K_b \quad (4)$$

2.4. Docking

The 3D structure of DNA was obtained from the Protein Data Bank (<http://www.rcsb.org/pdb/>) with the code: 423D [46]. The Chimera 1.8 software was used to remove waters, ions, and other molecules, and add hydrogens to the DNA [47]. The studied benzazoles were built in the software Avogadro 1.1.1 [48], following the semi-empirical PM6 geometry optimization using the program MOPAC2012 (<http://OpenMOPAC.net>) [49]. The derivatives and DNA in the pdbqt format were generated by AutoDockTools, where the ligands were considered flexible (with PM6 charges), and the DNA rigid (with Gasteiger charges) [50]. AutoDock Vina 1.1.1 program was used for the blind docking [51], using a gridbox of 603 Å (coordinates: x=-7.914, y=52.208, z=-0.176), an exhaustiveness of 50 and 1.0 Å of grid spacing. The results from docking were analyzed using the Accelrys Discovery Studio 3.5 software [52], and the conformer with the lowest binding free energy was selected as the best model of interaction.

2.5 Theoretical calculations

Quantum chemical calculations have been carried out by DFT and TD-DFT, CASSCF and CASPT2 methods in order to evaluate the photophysical and electronical properties of the amino and azido derivatives. The ground state geometries were optimized in DFT (Density Functional Theory) with the CAM-B3LYP functional and cc-pVDZ basis set [53]. Frequency calculations of the optimized structures were performed at the same level to confirm that the optimized structures are stationary points. The calculations of the vertical transitions were carried out using TDDFT with the CAM-B3LYP functional and jun-cc-pVTZ basis function. The CAM-B3LYP functional was employed because it presents the attributes of the B3LYP functional and long-range correction, which is crucial for a good description of excited states. The solvent effect was

considered in DFT and TDDFT calculations with PCM (Polarizable Continuum Model), and the solvents considered were acetonitrile (CH_3CN), dichloromethane (DCM) and ethanol (EtOH) [54]. Natural Transition Orbitals (NTO) was calculated because the molecules **4** and **6** showed more than one contribution to the first transition, hindering their qualitative description. NTOs drastically simplify the situation by providing a compact representation of the transition density matrix [55]. All the calculations described above were computed using the Gaussian 16 package [56]. In order to verify if the molecules present charge transfer, the analysis with the DCT descriptor [57] were carried out with the Multiwfn program [58].

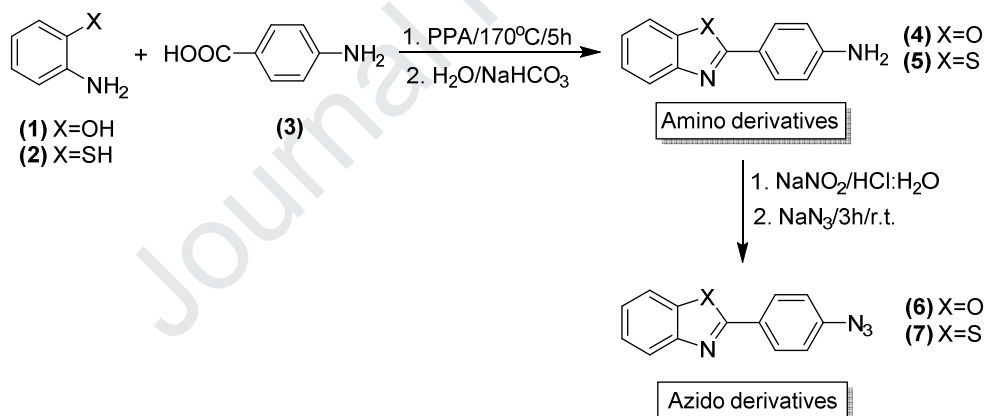
Multiconfigurational calculations were performed for azido benzoxazole **6** in order to investigate the lack of fluorescence of that molecule. The minima points and conical intersection (CoIn) point were optimized with an active space including 12 electrons and 12 orbitals (Figure 7) and state-averaged over three states (SA3-CASSCF(12,12)) with ANO-S-VDZP basis set. The orbitals included in the active space were six occupied and six virtual orbitals, wherein it were taken account the last six occupied orbitals (six occupied π orbitals) and the first six unoccupied orbitals (six virtual π orbitals). This active space was maintained during the subsequent geometry optimizations. Single point calculations using MS5-CASPT2(12,12) with ANO-L-VDZP basis set were performed for CASSCF geometries in order to improve the electronic correlation. The Minimal Energy Point (MEP) coordinate for molecule **6** was construct at SA3-CASSCF/cc-pVDZ level and energy corrected at MS5-CASPT2/ANO-L-VDZP level (CASPT2//CASSCF protocol). Baker criteria was used as geometry convergence criteria, *i.e.*, $1.0 e^{-6}$ and $3.0 e^{-4}$ with respect to the energy change and the norm of the gradient, respectively [59].

In all the CASSCF calculations, a level shift of 1.0 a.u. was used, and in the CASPT2 calculations. The IPEA modified H_0 with the shift parameter of 0.25 was also used [60,61]. The multiconfigurational (SA-CASSCF and MS-CASPT2) calculations were carried out with OpenMolcas package [62] and all orbitals were rendered with IboView program [63].

3. Results and Discussion

3.1. Synthesis

The amino benzazoles **4-5** were obtained by a condensation reaction between ortho-substituted anilines **1-2** and the p-aminobenzoic (**3**) in polyphosphoric acid (PPA) at 170°C for 5h as presented in Scheme 1 [64,65]. The progress of the reaction was monitored by TLC. The obtained precipitate was neutralized with NaHCO₃, filtered and dried at 60°C. The purification was performed by column chromatography using dichloromethane as eluent. The respective azides **6-7** were synthesized using the reaction of formation of diazonium salts from the previously prepared amines. The first step is the amino group diazotization at 0°C by reaction with sodium nitrite (NaNO₂) in aqueous hydrochloric acid. After the formation of the diazonium salt, sodium azide (NaN₃) was added to produce the respective azide. After 2h under stirring, the final solution was neutralized with NH₄OH, extracted with ethyl acetate and concentrated under reduced pressure to yield the azides **6-7**, which were used without further purification.



Scheme 1. Preparation of the amino (**4-5**) and azido benzazole (**6-7**) derivatives.

3.2. Photophysical properties

The photophysical investigation of the synthesized compounds was carried out using dichloromethane (DCM), ethanol (EtOH) and acetonitrile (ACN). The relevant data from the electronic ground and excited states characterization are summarized in Table 1. Figure 1 shows the UV-Vis spectra of the amino (**4-5**) and azido benzazole (**6-7**) derivatives.

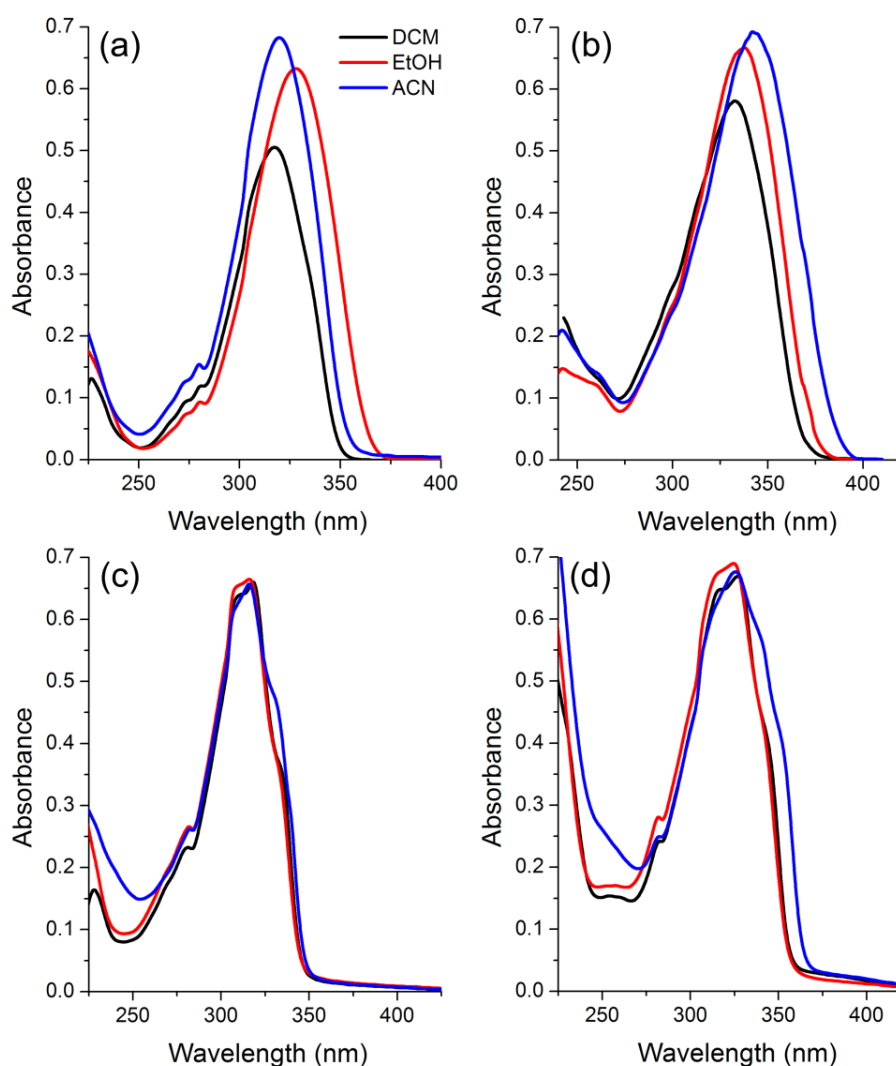


Figure 1. UV-Vis absorption spectra in solution of the amino benzazoles (a) **4** and (b) **5** and the respective azido derivatives (c) **6** and (d) **7**, where DCM: dichloromethane, EtOH: ethanol ACN: acetonitrile at a concentration $\sim 10^{-6}$ M for the amino and $\sim 10^{-5}$ M for the azido derivatives.

It can be observed that all studied compounds present absorption in the UV-A region. In both set of compounds, the heteroatom plays an important role, in which the sulfur derivatives present the absorption maxima located at higher wavelengths. This behavior was already observed in similar benzazoles and is related to the better electron delocalization allowed for this more electronegative heteroatom [5,6,8]. As already observed for benzazole analogues containing amino and azido moieties located at the same position, the azido derivatives

presented higher HOMO-LUMO energy gap, due to their lower electronic conjugation if compared to the amino ones [5].

In addition, the molar absorptivity coefficient values (ϵ) obtained by the UV-Vis spectroscopy allowed the obtention of the respective oscillator strengths (f_e), as well as the theoretical rate constants for emission (k_e^0) by applying a simplified version of the Strickler-Berg relations presented in Equations (4) and (5), respectively [66]. In Equation (5), $\bar{\nu}_0$ is the wavenumber (energy in $1/\lambda$ units) of the maximum of the absorption band. From k_e^0 , the pure radiative lifetime τ^0 was also calculated, defined as $1/k_e^0$ [67]. All these data are also summarized in Table 1.

$$f_e \approx 4.3 \times 10^{-9} \int \epsilon d\bar{\nu} \quad (4)$$

$$k_e^0 \approx 2.88 \times 10^{-9} \bar{\nu}_0^2 \int \epsilon d\bar{\nu} \quad (5)$$

The obtained molar absorptivity coefficient (ϵ) values $\sim 10^5 \text{ M}^{-1} \cdot \text{cm}^{-1}$, as well as the calculated radiative rate constants (k_e^0) ($\sim 10^8 \text{ s}^{-1}$) indicate for the amino (**4-5**) and azido (**6-7**) compounds, spin and symmetry allowed electronic transitions, which could be related to $^1\pi\pi^*$ transitions. Despite the higher values to ϵ , small values to the oscillator strength were found (<0.3). This result can be related to the size of the transition dipole which seems to be smaller than usually expected for compounds presenting fully electronic transitions. An almost constant radiative lifetime indicates that after the radiation absorption the molecular hybrids populate the same excited state.

Table 1. Photophysical data of the amino (**4-5**) and azido (**6-7**) derivatives by UV-Vis absorption spectroscopy, where ϵ_{\max} is the molar extinction coefficient at the absorption maxima ($\times 10^5 \text{ M}^{-1} \cdot \text{cm}^{-1}$), λ_{abs} is the absorption maxima (nm), f_e is the calculated oscillator strength, k_e^0 is the calculated radiative rate constant (10^8 s^{-1}) and τ^0 is the calculated pure radiative lifetime (ns).

Compound	Solvent	λ_{abs} (nm)	ϵ_{\max} ($\times 10^5 \text{ M}^{-1} \cdot \text{cm}^{-1}$)	f_e	k_e^0 (10^8 s^{-1})	τ^0 (ns)
4	Dichloromethane	317	0.81	0.16	1.58	6.33
	Ethanol	327	1.02	0.21	1.96	5.09
	Acetonitrile	320	1.09	0.22	2.14	4.67
5	Dichloromethane	333	0.64	0.20	1.81	5.52
	Ethanol	343	1.43	0.23	1.98	5.06
	Acetonitrile	338	1.05	0.28	2.44	4.10
6	Dichloromethane	317	0.51	0.14	1.37	7.31
	Ethanol	316	0.32	0.13	1.35	7.41
	Acetonitrile	316	0.62	0.14	1.38	7.23
7	Dichloromethane	327	0.59	0.15	1.45	6.92
	Ethanol	325	0.79	0.17	1.63	6.14
	Acetonitrile	325	0.55	0.17	1.62	6.18

The fluorescence emission curves presented in Figure 2 were obtained by exciting the compounds at the absorption maxima (Table 1). The relevant data is summarized in Table 2. All compounds presented a main fluorescence emission maximum in the UV-A to the violet region. In this sense, it can be observed that changes from amino to the azido moiety seem do not affect the emission maxima position. Once more, but with a higher magnitude, the sulfur compounds presented the emission maxima redshifted in contrast to the oxygenated analogues. All compounds presented relatively large Stokes shift ($\sim 5000\text{ cm}^{-1}$). Based on the chemical structure of these compounds and their relative rigidity, as well as the absence of a clear charge transfer character, the observed values can be probably related to organic solute-solvent interaction [68].

It is worth mentioning that the most significant difference between these compounds could be observed in the fluorescence quantum yield values. While derivatives containing the amino group show significantly higher values (~ 0.5), the azido derivatives presented values ten times smaller. As already observed in the literature, usually azide compounds are non-fluorescent, related to a photoinduced electron transfer (PET) mechanism ascribed to the presence of the $-\text{N}_3$ group. However, recent results indicate that a different mechanism than PET can tailor the fluorescence emission in such compounds [5]. In this sense, based on the theoretical results presented in this study and a study recently presented in the literature [69], the very weak fluorescence emission observed in these compounds could be related to the dissociative character of the S_1 state of these compounds. For a deeper discussion please see the theoretical calculation section.

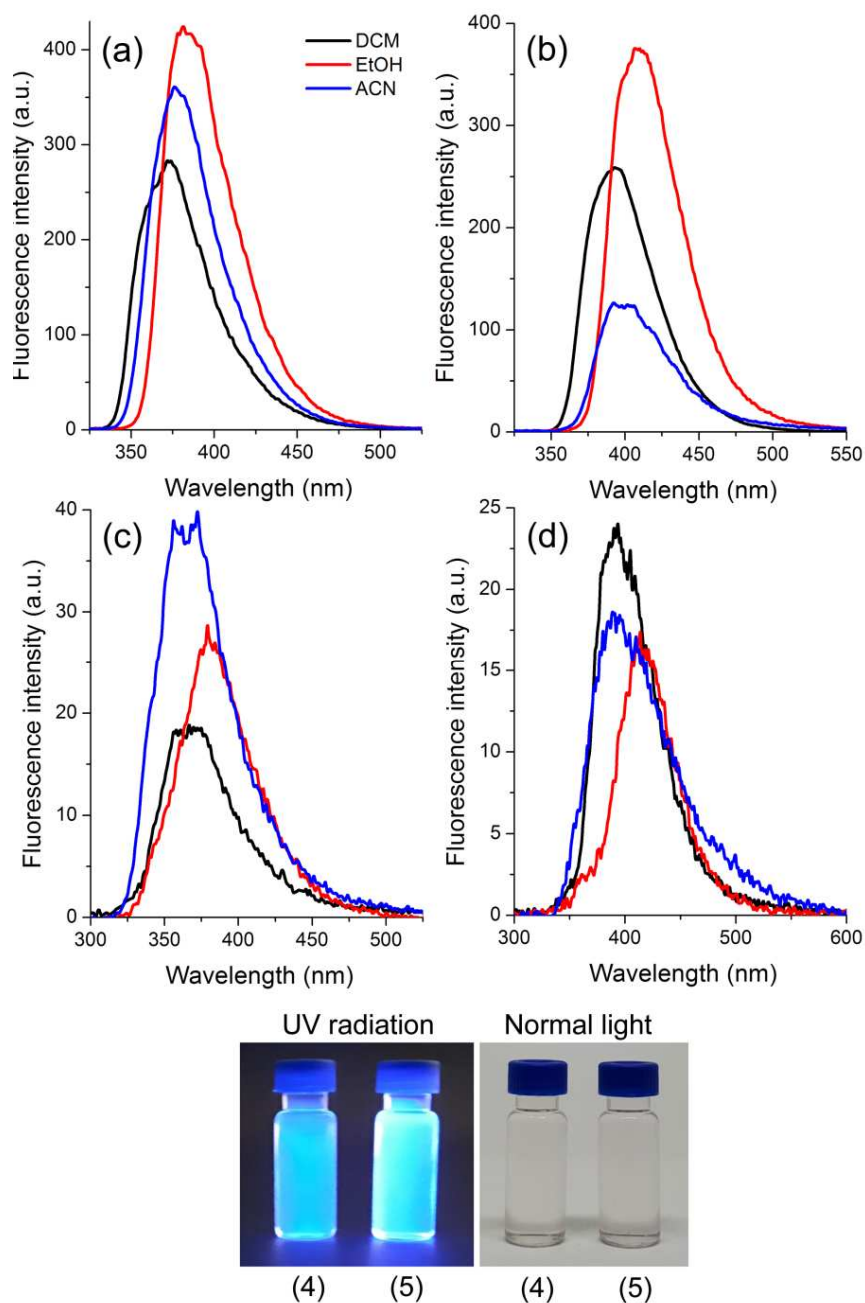


Figure 2. Steady-state fluorescence emission spectra in solution of the amino benzazoles (a) **4** and (b) **5** and the respective azido derivatives (c) **6** and (d) **7**, where DCM: dichloromethane, EtOH: ethanol ACN: acetonitrile at a concentration $\sim 10^{-6}$ M for the amino and $\sim 10^{-5}$ M for the azido derivatives. Exc/Em slits 3.0 nm/3.0 nm. Pictures of compounds **4** and **5** are also presented under normal light and UV-radiation (365 nm).

Table 2. Photophysical data from steady-state fluorescence emission spectroscopy of the amino (**4-5**) and azido (**6-7**) derivatives, where λ_{em} is the emission maxima, $\Delta\lambda_{ST}$ is the Stokes shift (nm/cm^{-1}) and ϕ_{FL} is the fluorescence quantum yield.

Compound	Solvent	λ_{em} (nm)	$\Delta\lambda_{ST}$ (nm/cm^{-1})	ϕ_{FL}
4	Dichloromethane	371	54/4592	0.58
	Ethanol	382	55/4403	0.51
	Acetonitrile	376	56/4654	0.48
5	Dichloromethane	393	60/4585	0.50
	Ethanol	410	67/4764	0.40
	Acetonitrile	401	63/4648	0.47
6	Dichloromethane	364	47/4073	0.05
	Ethanol	380	64/5330	0.04
	Acetonitrile	368	52/4472	0.08
7	Dichloromethane	392	65/5071	0.06
	Ethanol	415	90/6673	0.02
	Acetonitrile	390	65/5128	0.07

3.3 Theoretical calculations

The theoretical study has as its main goal the understanding how the intrinsic fluorescence quenching of the azido derivatives in comparison to their amino analogues. In this section, the photophysics features were investigated by TD-DFT and by multiconfigurational calculations. The discussion will be carried out for the amino benzoxazole **4** and the respective azide **6** as model compounds, since the sulfur analogues presented similar photophysical features. All the calculations resulting from these sulfur derivatives can be found in the ESI. Figure 3 shows the optimized geometries for the ground and first excited states of **4** and **6** in acetonitrile calculated with TD-DFT. Similar geometries were obtained in dichloromethane and ethanol (data not shown, see ESI).

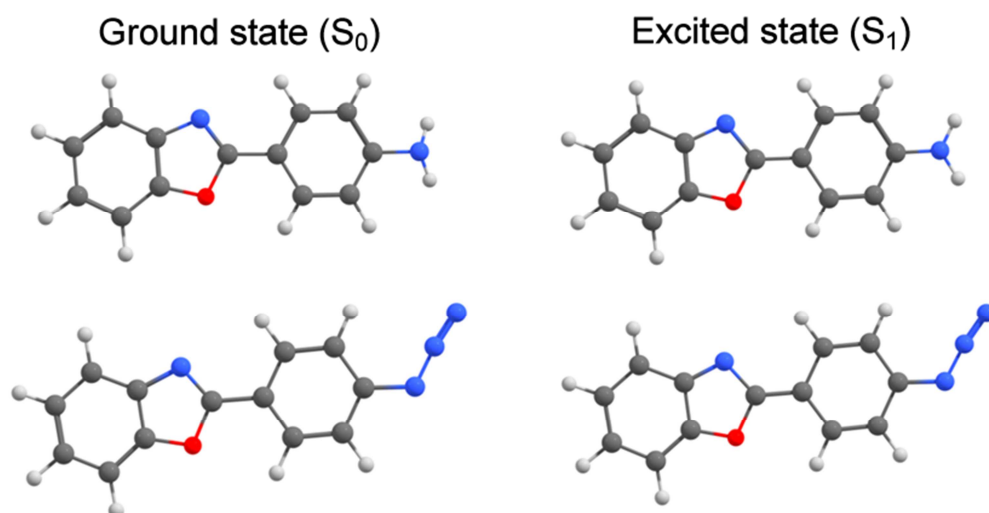


Figure 3. Optimized geometries of amino and azido benzazoles **4** (top) and **6** (bottom), respectively, calculated with CAM-B3LYP/cc-pVDZ level in acetonitrile.

It is possible to see that the geometries of the ground state are very similar of those in the first excited state for both molecules, indicating that these compounds do not present considerable geometry changes during the first electronic transition. Natural Transition Orbitals (NTO's) of the first electronic transition for the amino benzazole **4** and the respective azide **6**, including the solvent effect, are presented in Figure 4. These orbitals do not show a spatial separation in the transition, showing that there is only a local excitation. Furthermore, it is possible to confirm by analyzing the orbital coefficients that ${}^1\pi \rightarrow \pi^*$ transitions are occurring in both structures.

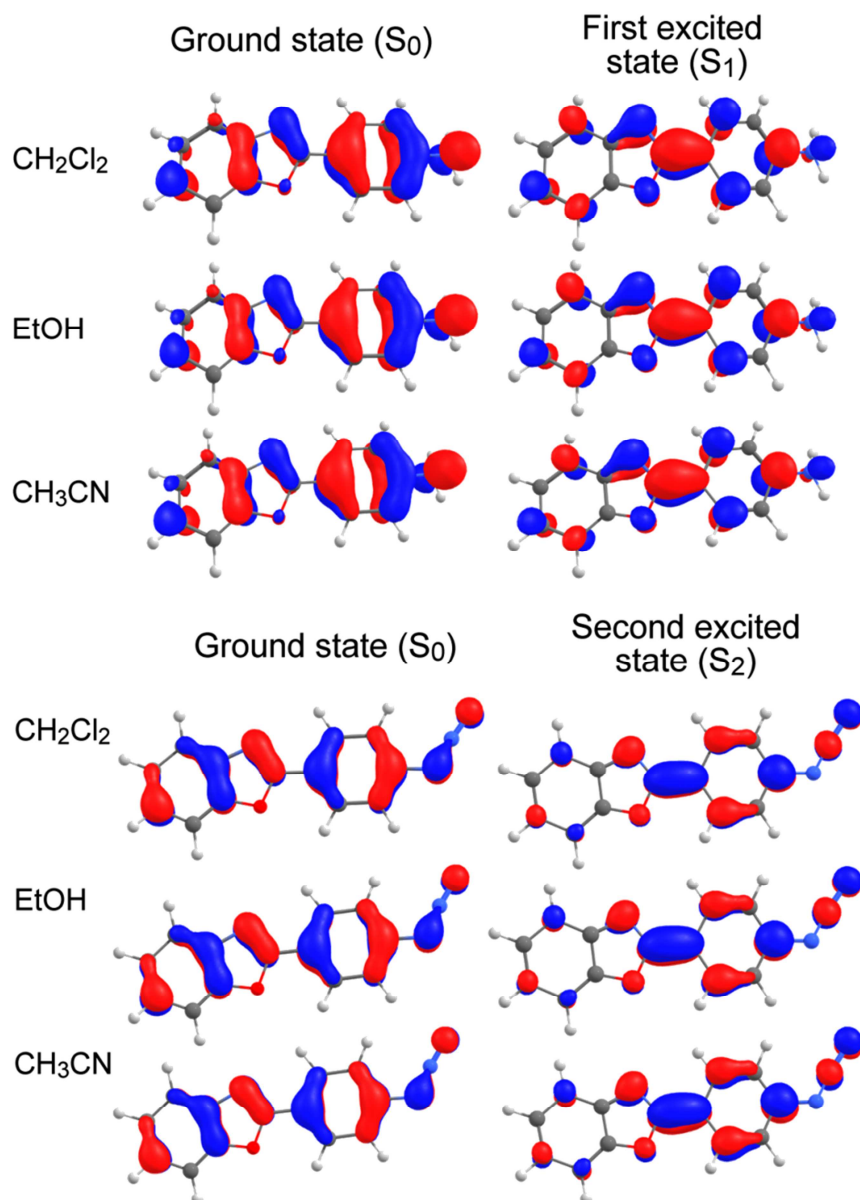


Figure 4. NTO's involved in the first transition for **4** (top) and **6** (bottom) computed at the CAM-B3LYP/jun-cc-pVTZ level in acetonitrile, dichloromethane and ethanol.

Table 3 shows the vertical transition analysis for amino benzazole **4** and the respective azido derivative **6**. It can be observed from the oscillator strength values, that the S_1 state for **4** is a bright state, and the S_2 , S_3 , S_4 and S_5 states are dark states, due to their small oscillator strengths. In this way, it can be predicted that the excitation undergoes from S_0 to S_1 , once S_1 presents the highest oscillator strength, i.e., the transition dipole moment is the highest for the $S_0 \rightarrow S_1$ transition. On the other hand, in the azide **6**, the state which

presents the highest oscillator strength is the S_2 , and S_1 , S_3 , S_4 and S_5 are the dark ones. Thus, it can be assumed for this derivative that the excitation goes from S_0 to S_2 . Taking the Kasha's rule into account, the azide derivative is excited to the S_2 state, and then, goes down to the S_1 state via internal conversion, due to the very close energies of both states.

Table 3. Absorption wavelength, oscillator strength (f_{osc}) and the main configuration of the lowest excited states calculated using CAM-B3LYP/jun-cc-pVTZ for amino and azido benzazoles **4** and **6**, respectively.

Compound	State	Character	λ_{abs}	f_{osc}
4	S_1	$1\pi\pi^*$	298.2	1.4820
	S_2	$1\pi\pi^*$	266.5	0.0220
	S_3	$1\pi\pi^*$	242.6	0.0680
	S_4	$1\pi\pi^*$	233.4	0.0013
	S_5	$1\pi\pi^*$	226.1	0.0241
6	S_1	$1\pi\pi^*$	305.2	0.0003
	S_2	$1\pi\pi^*$	299.3	1.2733
	S_3	$1\pi\pi^*$	258.5	0.0009
	S_4	$1\pi\pi^*$	244.1	0.0074
	S_5	$1\pi\pi^*$	234.9	0.0271

It can be found in the literature that the observed fluorescence quenching in molecules containing the azido moiety is due to Photoinduced Charge Transfer (PET) [70,71]. In order to verify if the azido derivative **6** also presents PET, the overlap integral between the centroids of charges (C^+ and C^-) before and after transition, obtained from the charge transfer diagnostic index (DCT), were computed in dichloromethane and ethanol. After the transition, the electronic density tends to be relocated considering the donor and acceptor groups in the molecule. The results of DCT analysis are shown in Figure 5. For both solvents, the centroids of charges before and after transition are localized in the same region with no displacement, excluding the charge transfer chance for this azide.

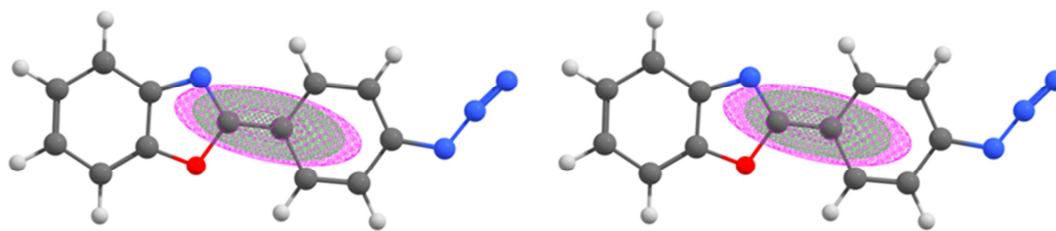


Figure 5. DCT overlap integral between centroids of charges obtained before and after the transition computed with the Multiwfn Program for azide **6** in dichloromethane (left) and ethanol (right).

Table 4 shows the theoretical absorption and emission wavelengths, the absorption and emission oscillator strengths and the dipole moment of the ground and excited states for molecules **4** and **6** in acetonitrile, dichloromethane and ethanol. The theoretical values of absorption and emission are relatively close to the experimental ones. It can be observed that the solvent does not affect the absorption and emission wavelengths, as experimentally observed.

As mentioned, the amine **4** presents a bright state at S_1 and the azide **6** at the S_2 for the ground state geometry. For this reason, the excitation energy of S_0 to S_1 was considered for the azide **4** and S_0 to S_2 energy for the molecule **6**. Despite the S_1 state is not a bright state for the molecule **6**, considering the Kasha's rule, it is possible to conclude that this state is quickly reached by internal conversion, and due to that, this state was optimized in order to obtain the theoretical emission values. As expect, the emission oscillator strength of amine **4** was high, explaining the high fluoresce emission experimentally observed. On the other hand, the emission oscillator strength of azide **6** was also high, an unexpected behavior due to the low fluoresce emission observed experimentally for this molecule. When the first excited state geometry was taken into account, the orbitals involved in the $S_1 \rightarrow S_0$ transition for molecule **6** were the HOMO and LUMO, and for the $S_2 \rightarrow S_0$ transition, the HOMO \rightarrow LUMO+1 prevails. On the other hand, when the geometry of the ground state was taken into account, the orbitals involved in the $S_0 \rightarrow S_1$ transition for molecule **6** were the HOMO and LUMO+1 and for the $S_0 \rightarrow S_2$ transition, the HOMO \rightarrow LUMO prevails. These results demonstrate an inversion between S_1 and S_2 states when the first excited state of molecule **6** has its

geometry relaxed. The orbitals involved in the $S_0 \rightarrow S_1$ and $S_0 \rightarrow S_2$ transitions of molecule **6** for the ground state geometry and first excited state geometry are shown in Figure 6. This figure clearly shows the inversion of the S_1 and S_2 states, wherein for the ground state geometry, the S_1 is the dark state and the S_2 the bright state, while for the first excited state geometry, the S_2 is the dark state and the S_1 is the bright state.

Journal Pre-proof

Table 4. Calculated photophysical data (CAM-B3LYP / jun-cc-pVTZ) for amine **4** and azide **6** in dichloromethane, ethanol and acetonitrile, where λ_{abs} and λ_{em} are the absorption and emission wavelengths (nm), μ_{S0} is the ground state dipole moment (Debye) and μ_{S1} is the first excited state dipole moment (Debye). The parameters λ_{abs} , f_{abs} and μ_{S0} were obtained from the ground state optimized geometry and the λ_{em} , f_{em} and μ_{S1} were obtained from the first excited state optimized geometry.

Molecule	Solvent	$\lambda_{\text{abs}} (\text{S0} \rightarrow \text{S1})$	f_{abs}	μ_{S0}	λ_{em}	$f_{\text{em}} (\text{S1} \rightarrow \text{S0})$	μ_{S1}
4	Dichloromethane	298.52	1.1735	4.2426	374.15	1.4573	8.0159
	Ethanol	298.41	1.1541	4.4120	380.04	1.50361	8.6454
	Acetonitrile	298.23	1.1482	4.4362	381.13	1.5117	8.7587
Molecule	Solvent	$\lambda_{\text{abs}} (\text{S0} \rightarrow \text{S2})$	f_{abs}	μ_{S0}	λ_{em}	$f_{\text{em}} (\text{S1} \rightarrow \text{S0})$	μ_{S1}
6	Dichloromethane	300.33	1.2991	1.6788	383.11	1.5618	2.0216
	Ethanol	299.55	1.2792	1.7098	385.88	1.6001	1.9816
	Acetonitrile	299.32	1.2733	1.7156	386.76	1.6074	1.9646

As mentioned, the amine **4** presents a bright state at S_1 and the azide **6** at the S_2 for the ground state geometry. For this reason, the excitation energy of S_0 to S_1 was considered for the azide **4** and S_0 to S_2 energy for the molecule **6**. Despite the S_1 state is not a bright state for the molecule **6**, considering the Kasha's rule, it is possible to conclude that this state is quickly reached by internal conversion, and due to that, this state was optimized in order to obtain the theoretical emission values. As expect, the emission oscillator strength of amine **4** was high, explaining the high fluoresce emission experimentally observed. On the other hand, the emission oscillator strength of azide **6** was also high, an unexpected behavior due to the low fluoresce emission observed experimentally for this molecule. Taking the first excited state geometry into account, the orbitals involved in the $S_1 \rightarrow S_0$ transition for molecule **6** were the HOMO and LUMO, and for the $S_2 \rightarrow S_0$ transition, the HOMO \rightarrow LUMO+1 prevails. These results demonstrate an inversion between S_1 and S_2 states when the first excited state of molecule **6** has its geometry relaxed. The orbitals involved in the $S_0 \rightarrow S_1$ and $S_0 \rightarrow S_2$ transitions of molecule **6** for the ground state geometry and first excited state geometry are shown in Figure 6. This figure clearly shows the observed inversion of the S_1 and S_2 states, wherein for the ground state geometry, the S_1 is the dark state and the S_2 the bright state, while for the first excited state geometry, the S_2 is the dark state and the S_1 is the bright state.

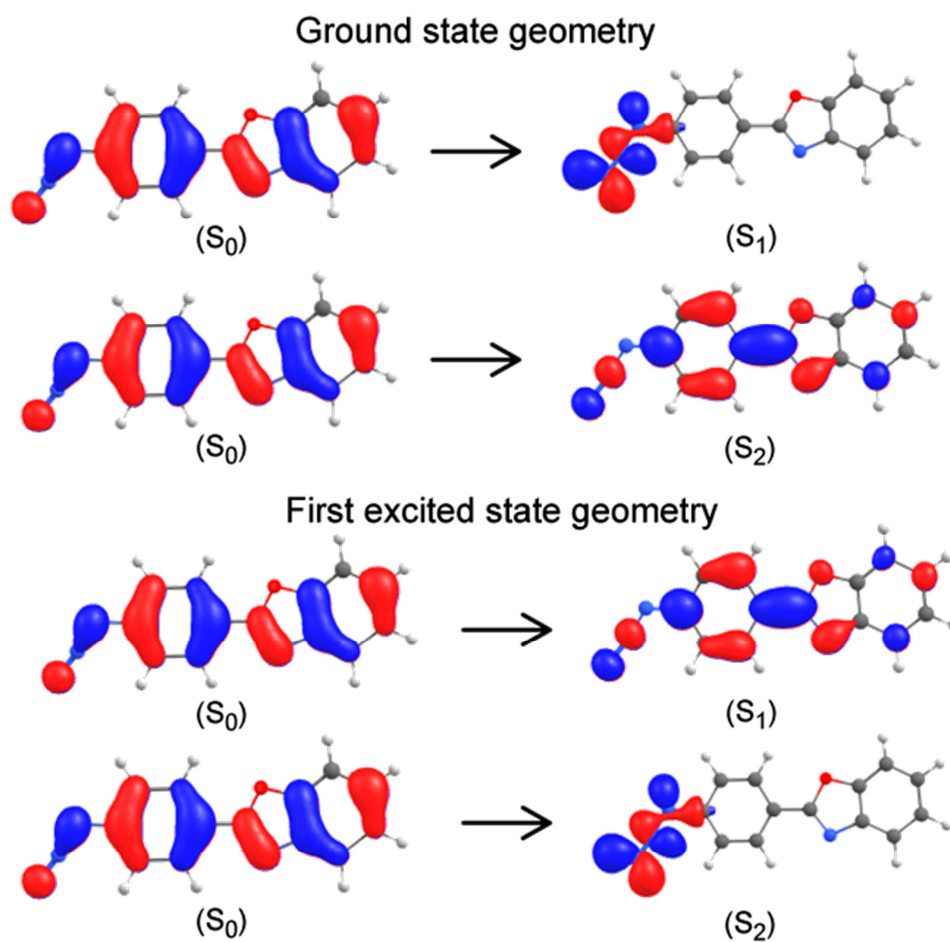


Figure 6. Kohn-Shan orbitals involved in the first and second transition for molecule **6** computed at the CAM-B3LYP/jun-cc-pVTZ level in acetonitrile for S_0 geometry (top) and S_1 geometry (bottom).

TDDFT results did not provide sufficient answers to explain the lack of fluorescence of molecule **6**. In order to complement the computational photophysical study, multiconfigurational calculations were also applied. In these calculations, it was used an active space including 12 electrons and 12 orbitals as shown in Figure 7.

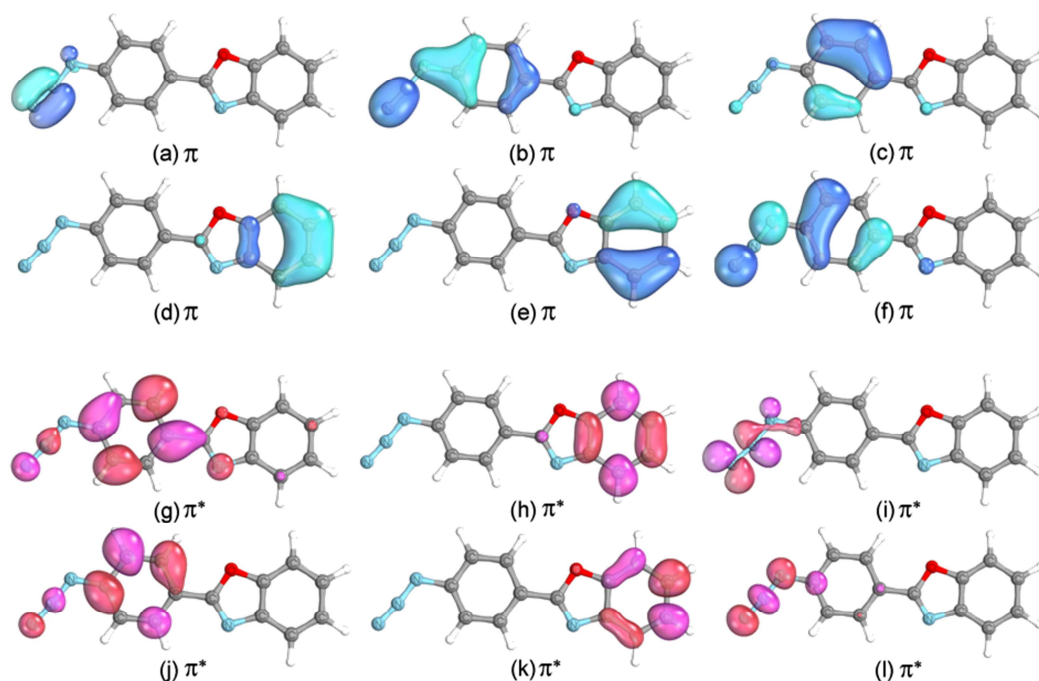


Figure 7. Active space of the azido benzazole **6** calculated with SA(4)-CASSCF(12,12)/ANO-S-VZDP.

Table 5. Vertical excitation energies (ΔE_{vert}), oscillator strength (f_{osc}) and character of the first four singlet states of azido derivative **6** with geometry optimized at SA3-CASSCF/ANO-S-VDZP and energy corrected at MS5-CASPT2/ANO-L-VDZP levels of theory.

State	Character	ΔE_{vert} (eV)	f_{osc}
S ₁	$^1\pi\pi^*$	4.280	0.000520
S ₂	$^1\pi\pi^*$	4.282	1.108350
S ₃	$^1\pi\pi^*$	5.662	0.002934
S ₄	$^1\pi\pi^*$	6.715	0.000334

The vertical transitions presented in Table 5 show that the S₁ and S₂ states energies are very close, and we can consider that are degenerate. In addition, the S₃ state is about 1.4 eV higher than S₂ and S₁, and S₄ state is about 2.5 eV higher than S₂ and S₁. Similar to the results obtained from TD-DFT, the oscillator strength of the S₂ state stands out from the other states and the S₁ and S₂ state presented a quite similar energy. In this sense, it can be supposed that the excitation undergoes from S₀ to S₂. The S₀→S₂ vertical

transition of molecule **6** had only one major contribution involving the **f** and **g** orbitals (Figure 7), this is a HOMO→LUMO transition, as well as observed in the TD-DFT results. Figure 8 shows the orbitals involved in the $S_0 \rightarrow S_1$ and $S_0 \rightarrow S_2$ transitions.

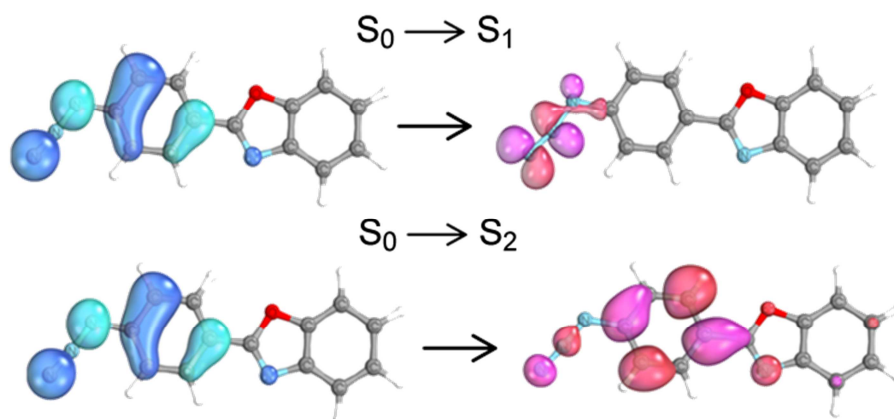


Figure 8. Orbitals involved in the first and second transition for molecule **6** computed at the CASSCF/ANO-L-VDZP level.

The orbital coefficients of CASSCF and TD-DFT involved in the $S_0 \rightarrow S_1$ and $S_0 \rightarrow S_2$ vertical transitions of molecule **6** (Figure 6 and 8, respectively) are similar, in other words, the dark state and the bright state computed at CASSCF/CASPT2 and TDDFT are very comparable. However, the CASPT2 predicts almost an absorption maximum of 290 nm (4.28 eV) for the bright state. On the other hand, the TDDFT value is 299 nm (4.15 eV) for the bright state and experiment result is 325-327 nm (3.81-3.79 eV). It is important to emphasize that the TD-DFT calculations take into account the solvent effects, while CASPT2 does not. Furthermore, we do not have gas-phase UV spectrum in order to compare with the theoretical results and take into account the solvent effects in CASPT2 calculations demands a lot of computational efforts. Moreover, take into account the similarity of the TDDFT and CASPT2 results, we can infer that the systems are been describing suitably with the active space employed. By analyzing the multiconfigurational calculations, we can predict that the S_2 state is populated after irradiation and, by internal conversion, it populates the S_1 state almost instantly. For these reasons, we performed geometry optimization of the S_1 state for molecule **6**, but this

calculation reached geometry wherein the S_0 and S_1 presented energies quite similar. In this way, a Minimal Energy Crossing Point (MECP) calculation was performed and thus, two points were obtained: the first one is related to the ground state minimum and the second one is related to the conical intersection (CoIn) point. No minimum in the S_1 surface close to the FC region was achieved, and because of that, it goes directly to the global minimum in the surface: the CoIn point. In order to support these results, a MEP coordinate from the S_1 state was constructed with CASPT2//CASSCF protocol, *i.e.*, all points were optimized at SA3-CASSCF(12,12)/cc-pVDZ level and energy corrected at MS5-CASPT2(12,12)/ANO-L-VDZP level (Figure 9).

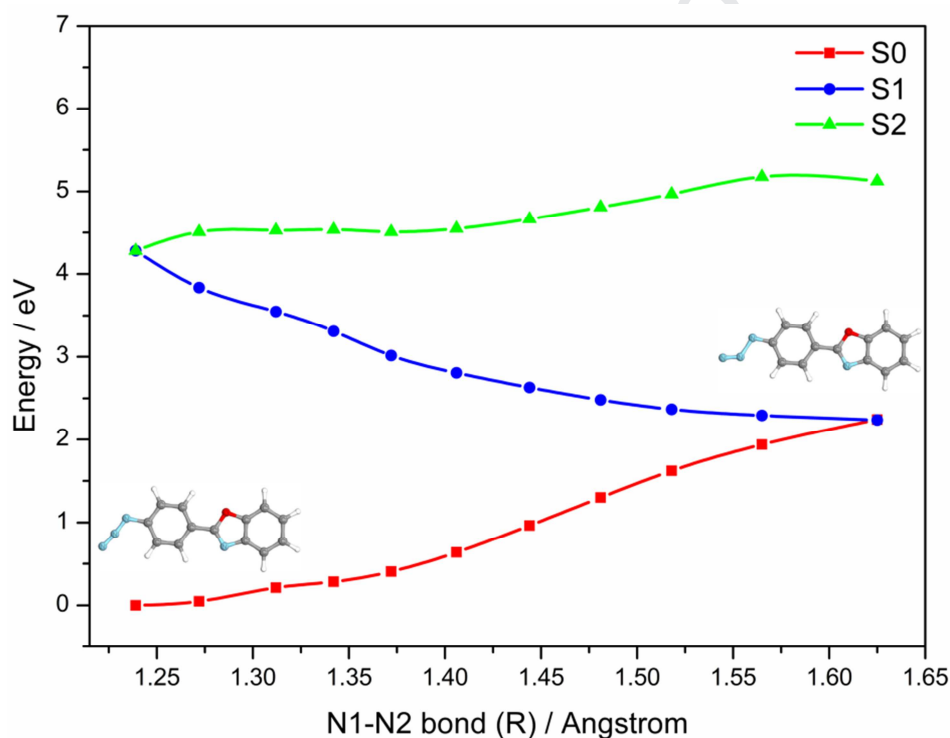


Figure 9. Potential energy curve for N1-N2 bond reaction coordinate construct by MEP for molecule **6** at SA3-CASSCF/cc-pVDZ level, energy corrected at MS5-CASPT2/ANO-L-VDZP level (CASPT2//CASSCF protocol).

Figure 9 shows that S_1 state is dissociative, since its curve presented no barrier to overcome. Thus, azide **6** reaches the CoIn and quickly relaxes back to the ground state. It explains the observed intrinsic quenching of fluorescence in this compound, since it decays by a CoIn,

which is a nonradioactive process. Furthermore, it is possible to verify that the electronic excitation of this system involves the occupation of an antibonding orbital on the azide group, leading to an increasing in the bond length N-N2. Due to this change, the azide **6** reaches to a Con point and returns to the ground state. The deactivation mechanism of this system involves degenerate points, such as the Con point. Here, it is important to emphasize once again that previous studies in the literature indicated that the fluorescence quenching in azido-based molecules were related to photoinduced charge transfer mechanism (PET). In contrast to the obtained results from TDDFT, the multiconfigurational methodology presented a notable difference between the geometries of the ground state and the global minimum of the first excited state, which is the conical intersection point. The main difference in the geometry occurs in the azide group, with increasing of the bond length between N1 and N2 in almost 0.4 Å at the conical point and the decreasing in the angle among the three nitrogen atoms. In order to understand why the S1 state in CASSCF/CASPT2 was dissociative while in TDDFT was not. It was carried out a geometry optimization of the S2 state of molecule **6** at CAM-B3LYP/cc-pVDZ level. This calculation reached a very similar geometry to the Con geometry as computed at CASSCF/CASPT2 level, as it is possible to see in the Figure 10. It was performed a single point calculation of that geometry and it presented a ΔE_{vert} of 0.57 eV (2171 nm) between S_0 and S_1 . Despite the low ΔE_{vert} , this value is very high to be considered a Con, however, degenerate points present multiconfigurational character, which cannot be properly described with monoconfigurational methods as TDDFT. In this way, it is necessary to use multiconfigurational methods in order to properly describe this phenomenon. The multiconfigurational methodologies (CASSCF and CASPT2) allowed explaining such particular photophysical behavior of this derivative. Thus, with the combination between the multiconfigurational and TDDFT results, we can conclude that the dark state involved in the excitation between the HOMO and the π orbitals, which involves the azido group (LUMO+1 of TDDFT calculations and the

LUMO+2 of CASPT2 calculations), is dissociative. When the geometry of the first excited state was relaxed at CAMB3LYP/cc-pVDZ level, it was observed the inversion of the S_1 and S_2 states. Due to this inversion, the S_1 does not reach the dissociative path, because the dark state becomes the S_2 , which are the dissociative one.

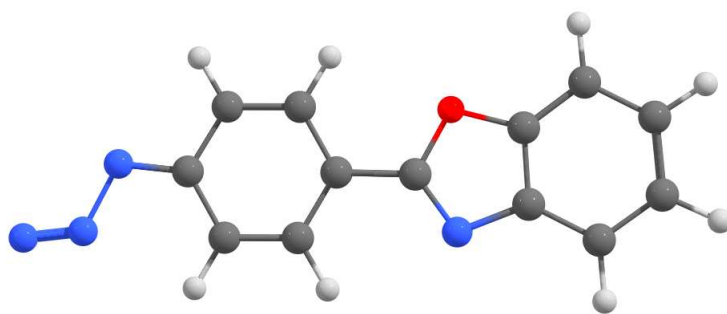


Figure 10. S_2 relaxed geometry of azido **6** calculated with CAM-B3LYP/cc-pVDZ level in acetonitrile.

The Figure 11 presents a qualitative deactivation pathway to the excited state of azide **6**, as well as, the orbitals involved in this process. In our proposal, the bright state (S_2) is populated after irradiation and by internal conversion the dark state (S_1) is reached. The dark state is dissociative and reaches a Con and returns to the ground state by a non-radioactive process.

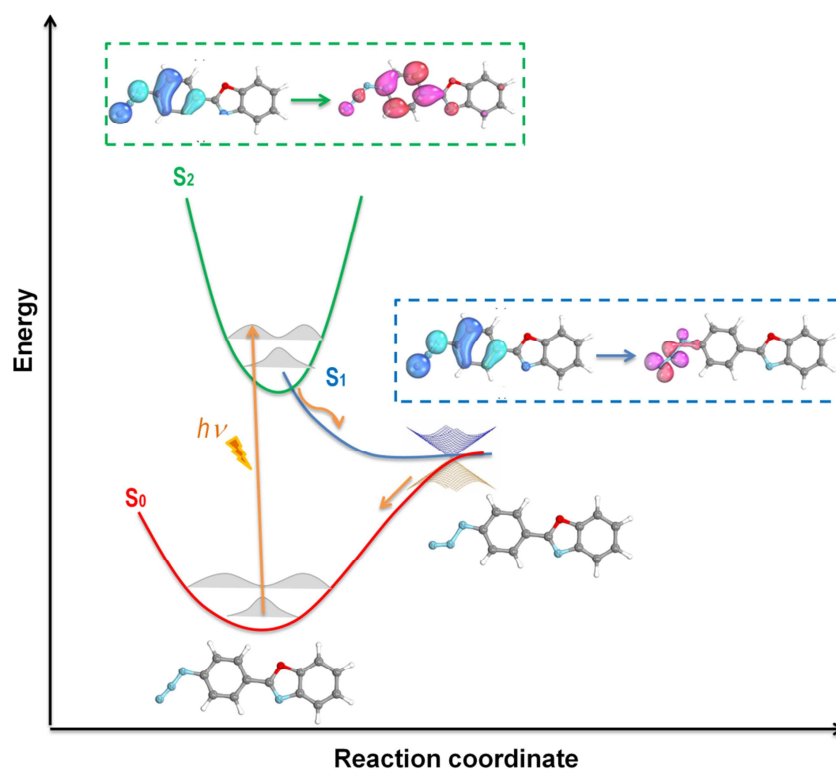


Figure 11. Schematic overview of the deactivation of the excited state of azide **6**.

However, despite the low emission yield, the azides also presented fluorescence emission. So, it can be presumed that after the bright state is populated, this state dissipates a small fraction of energy by fluorescence and the greatest part is transfer to the dark state and goes through the dissociative path. In addition, the experimental fluorescence emission maxima of 364-380 nm is similar to the theoretical ones (383-386 nm), obtained for the bright state calculated at CAM-B3LYP/jun-cc-pVTZ level.

3.4 CT-DNA interaction study

In order to better explore the structural and electronic features of these studied compounds, interaction assays with CT-DNA were also performed by UV-Vis and emission fluorescence titrations. The relevant data are summarized in Table 6. In Figure 12 shows the UV-Vis spectra of **5** at different amounts of CT-DNA (0 to 100 μM). It can be observed a slight change in the absorption intensity in the ultraviolet region. It is worth

mentioning that the UV-Vis CT-DNA titration spectra of all derivatives can be found in the ESI and presented a similar behaviour.

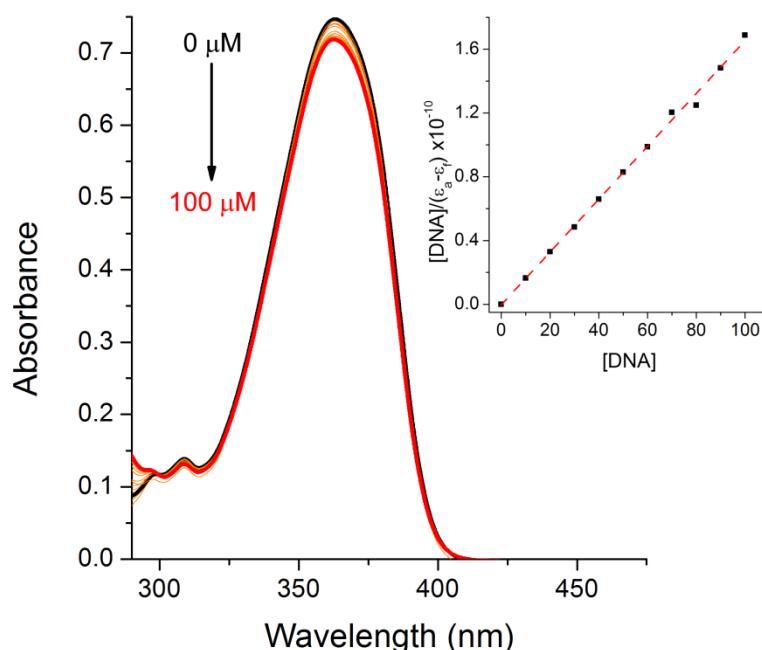


Figure 12. UV-Vis electronic absorption spectra of **5** with increasing CT-DNA concentrations ranging from 0 to 100 μM in DMSO(2%)/Tris-HCl pH 7.2 mixture solutions. The inset shows the linear correlation according to Equation (1) ($R^2=0.9985$).

Upon the CT-DNA addition, the amino derivative **5** presents a decrease in the absorbance intensity with no significant bathochromic shift. The observed hypochromic shift can probably be related to penetration or groove-interaction of the aromatic structure by hydrogen-bonding interactions with the DNA bases and heterocycle moieties. The rigid heterocycle structure of these derivatives would lead to stronger interaction with DNA, as previously reported for Peng and co-workers [72]. The interaction study also allowed obtaining the binding constants (K_b) of all studied compounds as summarized in Table 6. Higher values could be calculated ($\sim 10^6 \text{ M}^{-1}$) with the increasing order: **6**<**7**<**4**<**5**. These binding constant values are associated to the benzazoles-DNA complex stability, while the free energy indicates the spontaneity/non-spontaneity of compound-DNA binding process. In this sense, the calculated free-

energies were obtained as negative values (-8.50 to -9.10 Kcal·mol⁻¹), indicating the spontaneity of the interaction between the benzazoles and the DNA, with compounds **4** and **5** binding to DNA more spontaneously if compared to **6** and **7**.

In the fluorescence emission analysis, competitive-binding EB-DNA experiments were also used to determine the displacement of the intercalating agent ethidium bromide (EB) from acid nucleic. This study was performed in order to provide additional information about the binding affinity of the synthesized derivatives **4-7** with CT-DNA. In this way, the fluorescence emission of compound **7** was monitored increasing the fluorophore concentration at a fixed concentration of CT-DNA pre-treated with EB, as depicted in Figure 13. The EB-DNA emission fluorescence spectra of other derivatives are listed in the ESI.

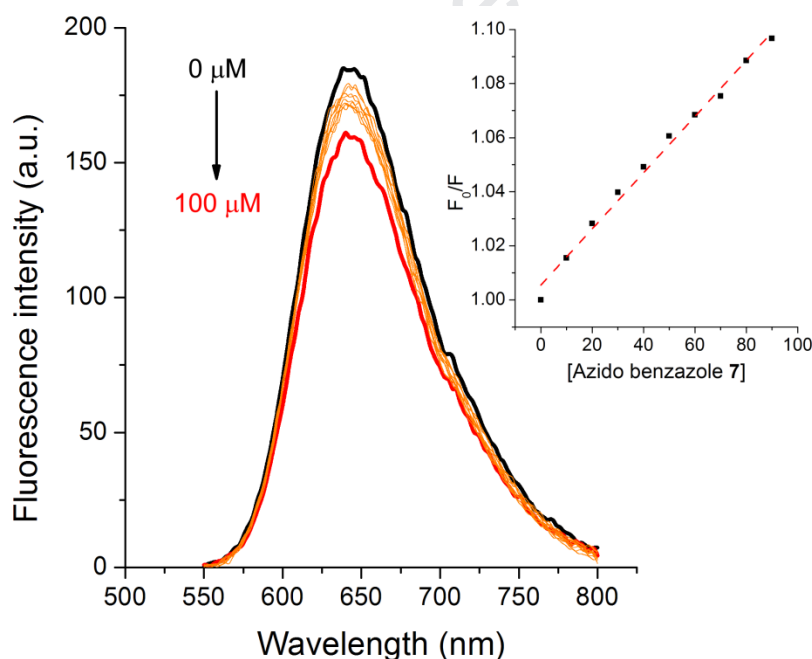


Figure 13. Fluorescence emission spectra of EB bound to CT-DNA in the presence of **7** in a DMSO(2%)/Tris-HCl pH 7.2 mixture at $\lambda_{exc}=510$ nm. The inset shows the plot of F_0/F versus the concentration of compound **7** according to Equation (2) ($R^2=0.9959$).

As it can be observed, the EB-DNA competition experiment shows an intense fluorescence emission located at 642 nm (λ_{em}) under excitation at 510

nm (λ_{exc}) ascribed to the ethidium bromide dye emission. It can also be observed that the emission spectra of EB bound to CT-DNA in absence of the compound **7** (black line). After addition of **7** to the DNA with ethidium bromide (EB), the nucleic acid-induced emission of EB was seen to decrease its intensity. This result demonstrates a weak fluorescence quenching of the EB-DNA adduct, as estimated by the K_{SV} values presented in Table 6. This behaviour can be attributed to the competition of the benzazoles with EB over binding to the bases pair of CT-DNA (intercalation mode). In addition, the inset of Figure 10 shows the Stern-Volmer plot, where a linear correlation was obtained between F_0/F versus the concentration of **7**. High values were obtained to the quenching constant rate (k_q), which were higher than the diffusion rate constant ($k_{diff} \sim 7.40 \times 10^9 \text{ M}^{-1} \cdot \text{s}^{-1}$ at 298 K, according to Smoluchowski-Stokes-Einstein theory). This result indicates a static interaction mechanism between the benzazoles derivatives and EB-DNA [73], which takes place via ground state association, following to the moderate DNA-binding apparent constants (K_{app}) (Table 6).

Table 6. CT-DNA-binding data from UV-Vis absorption and fluorescence emission of derivatives 4-7.

Compound	CT-DNA absorption				EB-DNA emission			
	<i>H</i> (%) ^a	$\Delta\lambda$ (nm) ^b	K_b (M ⁻¹) ^c	ΔG° (kcal·mol ⁻¹)	<i>Q</i> (%) ^d	K_{SV} (M ⁻¹) ^e	k_q (M ⁻¹ ·s ⁻¹) ^f	K_{app} (M ⁻¹) ^g
4	4.21	0.0	2.98x10 ⁶	- 8.83	6.90	7.81x10 ²	3.39x10 ¹⁰	2.96x10 ⁴
5	3.75	0.0	4.55x10 ⁶	-9.08	7.97	4.47x10 ²	1.94x10 ¹⁰	3.70x10 ⁴
6	3.56	0.0	1.72x10 ⁶	-8.50	5.22	5.18x10 ²	2.25x10 ¹⁰	2.12x10 ⁴
7	7.26	0.0	2.60x10 ⁶	-8.75	13.69	1.04x10 ³	4.52x10 ¹⁰	2.47x10 ⁴

^a $H(\%) = (Abs_{initial} - Abs_{final}) / (Abs_{initial}) \times 100$;

^b $\Delta\lambda(\text{nm}) = \lambda_{final} - \lambda_{initial}$;

^cBinding constant by UV-Vis CT-DNA analysis;

^d $Q(\%) = (Emission_{initial} - Emission_{final}) / (Emission_{initial}) \times 100$;

^eStern-Volmer quenching EB-DNA constant (K_{SV}) by steady-state emission spectra;

^fStern-Volmer rate quenching EB-DNA constant (k_q) by steady-state emission spectra;

^gDNA-binding apparent constant (K_{app});

3.5 Docking

To simulate the interactions between the amino (**4-5**) and the azido (**6-7**) derivatives with the CT-DNA, the crystal structure with a mixed nucleotide sequence were selected [d(ACCGACGTCGGT)₂] (PDB ID: 423D) [74]. According to the molecular docking, all the molecules interact in the minor groove of the DNA, as presented in Figure 14. The molecules **4**, **5**, and **7** bind in the same site, between the nucleotides dA5 and dG4 from the DNA strand A, and dT20, dC21, dG22 from the DNA strand B. The amino derivatives **4** and **5** showed very similar binding pose, interacting with dG22 and dA5 via hydrophobic π - π stacking and H-bonds with the amino moiety from dG4, according to the experimental analysis. However, molecule **7** showed a different binding pose when compared with **4** and **5**. The azido derivative **7** interacts with the dG22 and dA5 by π - π stacking. On the other hand, the molecule **6** interacts in the region between the nucleotides dG7, dT8 and dC9 from the DNA strand A, and dG19 and dT20 from the DNA strand B, making H-bonds with the amino group from dG7 and hydrophobic π - π stacking with the purine ring from dG19. In addition, according to the docking simulations, it can be observed that O or N atoms from the oxazole/thiazole ring play an important role in the bind with the DNA via H-bonds. Moreover, it can be observed that the amino group does not change the binding pose of **4** and **5**, while the azido group changes the binding mode of **6** and **7**, respectively. The predicted binding free energy (ΔG_{bind}) indicated that both compounds interact with the DNA spontaneously and with similar energy (**4**: $-6.8 \text{ kcal}\cdot\text{mol}^{-1}$; **5**: $-6.7 \text{ kcal}\cdot\text{mol}^{-1}$; **6**: $-7.1 \text{ kcal}\cdot\text{mol}^{-1}$; **7**: $-7.0 \text{ kcal}\cdot\text{mol}^{-1}$). The docking results obtained are in accordance with the literature and the experimental data, were previous studies have been indicated that benzoxazole and/or benzothiazole derivatives interact in the minor groove of the DNA [75-79].

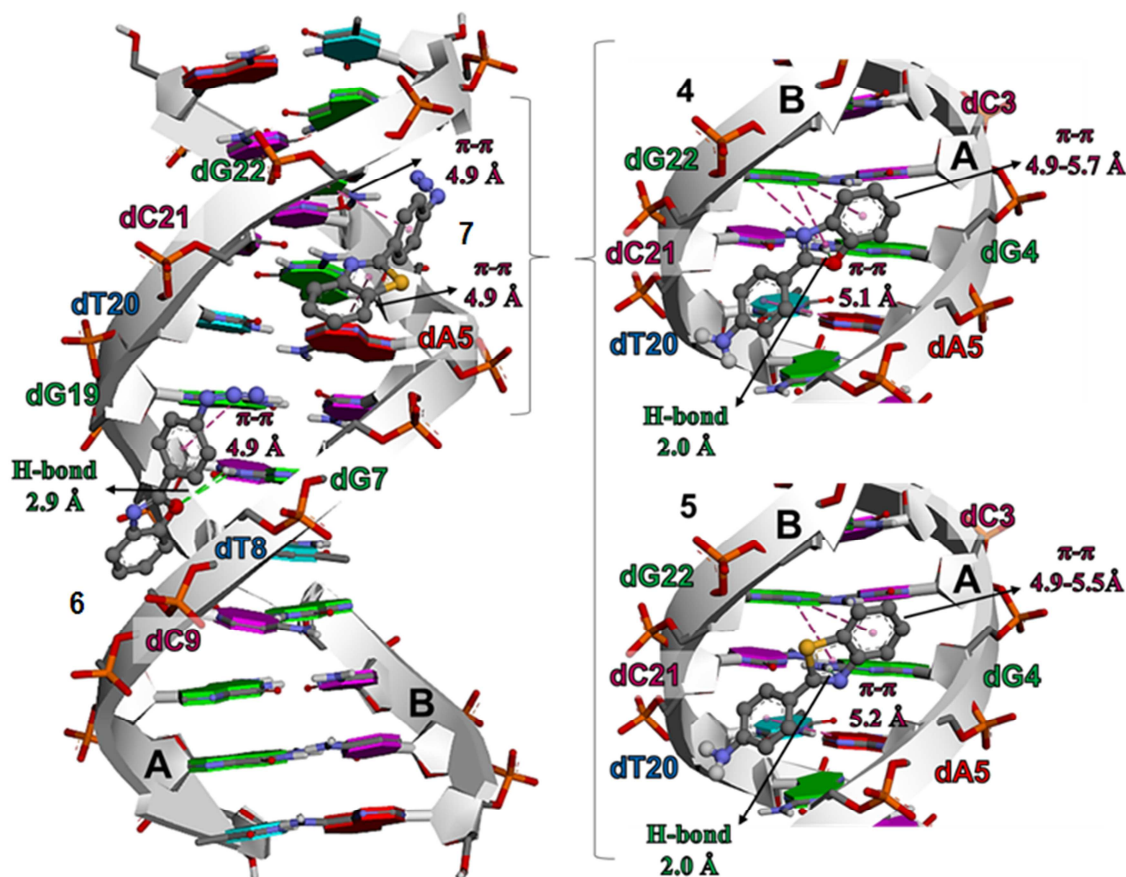


Figure 14. Docking simulation between the amino (4-5) and the azido (6-7) derivatives with DNA. The DNA rings in red, blue, pink and green represent the deoxyadenosine (dA), deoxythymidine (dT), deoxycytidine (dC) and deoxyguanosine (dG), respectively. H-bonds and π - π stacking interactions are shown in green and pink dot lines, respectively.

4. Conclusion

In summary, this work presented the synthesis of two azido benzazole obtained via diazonium salts formation from the respective amino precursors followed by addition of sodium azide in good yields. Both set of compounds presented absorption maxima located in the UV region, ascribed to fully spin and symmetry allowed electronic transitions. The studied compounds presented fluorescence emission maxima located in the UV-A to the violet region with relatively large Stokes shift, probably due to solute-solvent interaction. The azido derivatives presented significantly lower fluorescence intensities if compared to the amino compounds. Despite the indication in the literature that a photoinduced electron transfer (PET) mechanism can take place in these

azido compounds, theoretical calculations performed in this study related the observed lower fluorescence intensity to the dissociative character of the first excited state present in these structures. DNA-binding analysis by absorption and emission spectroscopies showed that all studied benzazole derivatives presented strong interactions with CT-DNA, which could be attributed to π -stacking and/or hydrogen-bonding interactions, confirmed by molecular docking calculation. By DCT analysis, it was not observed charge transfer in the excited state for molecules containing the azide moiety in their structure. In this sense, charge transfer, and consequently PET could not explain their very low fluorescence intensities. However, taking the azido **6** as a model, the high level multiconfigurational calculations showed that the observed intrinsic fluorescence quenching was caused by the dissociative character of its first excited state, which reaches to a conical intersection between S_0/S_1 , and through this point, it relaxes non-radiatively back to the ground state.

Conflict of interests

The authors have declared no conflict of interest.

Acknowledgements

The authors would like to acknowledge FAPERGS (17/2551-0000968-1), CNPq (409855/2018-9, 409150/2018-5 and 304711/2018-7) and Coordenação de Aperfeiçoamento de Pessoal de Nível Superior - Brasil (CAPES) - Finance Code 001 for the financial support. Special thanks for M.Sc. Luana Silva for HRMS data.

References

-
- [1] W.H. Lin, W.C. Wu, M. Selvaraju, C.M. Sun, One-pot synthesis of benzazoles and quinazolinones via iron pentacarbonyl mediated carbonylation of aryl iodides under microwave irradiation, *Org. Chem. Front.* 4 (2017) 392-397 and references cited therein.
- [2] A.R. Katritzky, C.A. Ramsden, E.F.V. Scriven, R.J.K. Taylor, *Comprehensive Heterocyclic Chemistry III*, 2008, pages xxi-xxix.

- [3] A.R. Katrizky (Editor) In: *Advances in Heterocyclic Chemistry*, Volume 76, 1st Edition, Academic Press.
- [4] T. Kroetz, M.C. dos Santos, R. Beal, G.M. Zanotto, F.S. Santos, F.C. Giacomelli, P.F.B. Gonçalves, V.R. de Lima, A.G. Dal-Bó, F.S. Rodembusch, Proton transfer fluorescent secondary amines. Synthesis, photophysics, theoretical calculation and preparation of photoactive phosphatidylcholine-based liposomes, *Photochem. Photobiol. Sci.* 18 (2019) 1171-1184.
- [5] C.B. da Silva, E.S. Gil, F.S. Santos, A.M. Morás, L. Steffens, P.F.B. Gonçalves, D.J. Moura, D.S. Lüdtkke, F.S. Rodembusch, Proton-transfer based azides with fluorescence off–on response for detection of hydrogen sulfide. an experimental, theoretical and bioimaging study, *J. Org. Chem.* 83 (2018) 15210-15224.
- [6] G. Wiethaus, J.M. Toldo, F.S. Santos, R.C. Duarte, P.F.B. Gonçalves, F.S. Rodembusch, Experimental and theoretical investigation of long-wavelength fluorescence emission in push-pull benzazoles: intramolecular proton transfer or charge transfer in the excited state?, *Phys. Chem. Chem. Phys.* 21 (2019) 4408-4420.
- [7] C.B. da Silva, T. Kroetz, F.S. Santos, F.S. Rodembusch, Synthesis and photophysical characterisation of proton transfer-based thiourea derivatives. potential application as a colorimetric naked-eye chemosensor for fluoride detection in solution, *J. Braz. Chem. Soc.* 28 (2017) 1830-1841.
- [8] F.S. Santos, N.G. Medeiros, R.F. Affeldt, R.D. Duarte, S. Moura, F.S. Rodembusch, Small heterocycles as highly luminescent building blocks in the solid state for organic synthesis, *New J. Chem.* 40 (2016) 2785-2791.
- [9] R.F. Affeldt, A.C.A. Borges, D. Russowsky, F.S. Rodembusch, Synthesis and fluorescence properties of benzoxazole-1,4-dihydropyridine dyads achieved by multicomponent reaction, *New J. Chem.* 38 (2014) 4607-4614.
- [10] R.D. Viirre, G. Evindar, R.A. Batey, Copper-catalyzed domino annulation approaches to the synthesis of benzoxazoles under microwave-accelerated and conventional thermal conditions, *J. Org. Chem.* 73 (2008) 3452-3459.
- [11] P. Saha, T. Ramana, N. Purkait, M.A. Ali, R. Paul, T. Punniyamurthy, Ligand-free copper-catalyzed synthesis of substituted benzimidazoles, 2-

aminobenzimidazoles, 2-aminobenzothiazoles, and benzoxazoles. *J. Org. Chem.* 74 (2009) 8719-8725.

[12] J. Peng, M. Ye, C. Zong, F. Hu, L. Feng, X. Wang, Y. Wang, C. Chen, Copper-catalyzed intramolecular c–n bond formation: a straightforward synthesis of benzimidazole derivatives in water. *J. Org. Chem.* 76 (2011) 716-719.

[13] H. Baars, A. Beyer, S.V. Kohlhepp, C. Bolm, Transition-metal-free synthesis of benzimidazoles mediated by KOH/DMSO. *Org. Lett.* 16 (2014) 536-539.

[14] S.S. Panda, M.A. Ibrahim, A.A. Oliferenko, A.M. Asiri, A.R. Katritzky, Catalyst-free facile synthesis of 2-substituted benzothiazoles. *Green Chem.* 15 (2013) 2709-2712.

[15] Y.K. Bommegowda, G.S. Lingaraju, S. Thamas, K.S.V. Kumar, C.S.P. Kumara, K.S. Rangappa, M.P. Sadashiva, Weinreb Amide as an efficient reagent in the one pot synthesis of benzimidazoles and benzothiazoles. *Tetrahedron Lett.* 54 (2013) 2693-2695.

[16] Y. Sun, H. Jiang, W. Wu, W. Zeng, X. Wu, Copper-catalyzed synthesis of substituted benzothiazoles via condensation of 2-aminobenzenethiols with nitriles. *Org. Lett.* 15 (2013) 1598-1601.

[17] C. Zhang, L. Zhang, N. Jiao, Catalyst free approach to benzimidazoles using air as the oxidant at room temperature. *Green Chem.* 14 (2012) 3273-3276.

[18] S. Samanta, S. Das, P. Biswas, Photocatalysis by 3,6-disubstituted-s-tetrazine: visible-light driven metal-free green synthesis of 2-substituted benzimidazole and benzothiazole. *J. Org. Chem.* 78 (2013) 11184-11193.

[19] S. Chen, M.S. Hossain, F.W. Foss Jr., Bioinspired oxidative aromatizations: one-pot syntheses of 2-substituted benzothiazoles and pyridines by aerobic organocatalysis. *ACS Sustainable Chem. Eng.* 1 (2013) 1045-1051.

[20] H. Chen, Y. Zhang, L. Li, J.G. Han, Probing ligand-binding modes and binding mechanisms of benzoxazole-based amide inhibitors with soluble epoxide hydrolase by molecular docking and molecular dynamics simulation. *J. Phys. Chem. B* 116 (2012) 10219-12233.

- [21] A. Sankaranarayanan, G. Raman, C. Busch, T. Schultz, P.I. Zimin, J. Hoyer, R. Köhler, H. Wulff, Naphtho[1,2-d]thiazol-2-ylamine (SKA-31), a new activator of KCa₂ and KCa_{3.1} potassium channels, potentiates the endothelium-derived hyperpolarizing factor response and lowers blood pressure. *Mol. Pharmacol.* 75 (2009) 281-295.
- [22] H. Razavi, S.K. Palaninathan, E.T. Powers, R.L. Wiseman, H.E. Purkey, N.N. Mohamedmohaideen, S. Deechongkit, K.P. Chiang, M.T. Dendle, J.C. Sacchettini, J.W. Kelly, Benzoxazoles as transthyretin amyloid fibril inhibitors: synthesis, evaluation, and mechanism of action. *Angew. Chem. Int. Ed.* 42 (2003) 2758-2761.
- [23] T. Grandi, F. Sparatore, C. Gnerre, P. Crivori, P.A. Carrupt, B. Testa, Monoamine oxidase inhibitory properties of some benzazoles: structure-; activity relationships, *AAPS PharmSci.* 1 (1999) 1-4.
- [24] N.P. Lad, Y. Manohar, M. Mascarenhas, Y.B. Pandit, M.R. Kulkarni, R. Sharma, K. Salkar, A. Suthar, S.S. Pandit, Methylsulfonyl benzothiazoles (MSBT) derivatives: search for new potential antimicrobial and anticancer agents, *Bioorg. Med. Chem. Lett.* 27 (2017) 1319-1324.
- [25] N. Karali, O. Güzel, N. Ozsoy, S. Ozbey, A. Salman, Synthesis of new spiroindolinones incorporating a benzothiazole moiety as antioxidant agents, *Eur. J. Med. Chem.* 45 (2010) 1068-1077.
- [26] M.J. Akhtar, A.A. Khan, Z. Ali, R.P. Dewangan, M. Rafi, M.Q. Hassan, M.S. Akhtar, A.A. Siddiqui, S. Partap, S. Pasha, M.S. Yar, Synthesis of stable benzimidazole derivatives bearing pyrazole as anticancer and EGFR receptor inhibitors, *Bioorg. Chem.* 78 (2018) 158-169.
- [27] P.P. Netalkar, S.P. Netalkar, S. Budagumpi, V.K. Revankar, Synthesis, crystal structures and characterization of late first row transition metal complexes derived from benzothiazole core: anti-tuberculosis activity and special emphasis on DNA binding and cleavage property, *Eur. J. Med. Chem.* 79 (2014) 47-56.
- [28] E. Meltzer-Mats, G. Babai-Shani, L. Pasternak, N. Uritsky, T. Getter, O. Viskind, J. Eckel, E. Cerasi, H. Senderowitz, S. Sasson, A. Gruzman, Synthesis and mechanism of hypoglycemic activity of benzothiazole derivatives, *J. Med. Chem.* 56 (2013) 5335-5350.

- [29] M.A. Azam, L. Dharanya, C.C. Mehta, S. Sachdeva, Synthesis and biological evaluation of some novel pyrazolopyrimidines incorporating a benzothiazole ring system, *Acta Pharm.* 63 (2013) 19-30.
- [30] S.A.J. Sulaiman, G.S. Al-Rasbi, O.K. Abou-Zied, Photophysical properties of hydroxyphenyl benzazoles and their applications as fluorescent probes to study local environment in DNA, protein and lipid, *Luminescence* 31 (2016) 614-625.
- [31] O.K. Abou-Zied, R. Jimenez, F.E. Romesberg, A phototautomerizable model DNA base pair, *J. Am. Chem. Soc.* 123 (2001) 4613-4614.
- [32] H. Wang, H. Zhang, O.K. Abou-Zied, C. Yu, F.E. Romesberg, M. Glasbeek, Femtosecond fluorescence upconversion studies of excited-state proton-transfer dynamics in 2-(2'-hydroxyphenyl)benzoxazole (HBO) in liquid solution and DNA, *Chem. Phys. Lett.* 367 (2003) 599-608.
- [33] F.Y. Dupradeau, D.A. Case, C. Yu, R. Jimenez, F.E. Romesberg, Differential solvation and tautomer stability of a model base pair within the minor and major grooves of DNA, *J. Am. Chem. Soc.* 127 (2005) 15612-15617.
- [34] O.K. Abou-Zied, Spectroscopy of hydroxyphenyl benzazoles in solution and human serum albumin: detecting flexibility, specificity and high affinity of the warfarin drug binding site, *RSC Adv.* 3 (2013) 8747-8755.
- [35] O.K. Abou-Zied, Revealing the ionization ability of binding site i of human serum albumin using 2-(2'-hydroxyphenyl)benzoxazole as a pH sensitive probe, *Phys. Chem. Chem. Phys.* 14 (2012) 2832-2839.
- [36] W. Yan, L. Xu, W. Ma, L. Liu, L. Wang, H. Kuang, C. Xu, Pyramidal sensor platform with reversible chiroptical signals for DNA detection, *Small* 10 (2014) 4293-4297.
- [37] T. Galán, B. Prieto-Simón, M. Alvira, R. Eritja, G. Götz, P. Bäuerle, J. Samitier, Label-free electrochemical DNA sensor using "click"-functionalized PEDOT electrodes, *Biosens. Bioelectron.* 74 (2015) 751-756.
- [38] W.L.F. Armarego, In: *Purification of Laboratory Chemicals*, 5th ed.; Elsevier Academic Press: Cornwall, UK, **2003**.
- [39] C. Würth, M. Grabolle, J. Pauli, M. Spieles U. Resch-Genger, Relative and absolute determination of fluorescence quantum yields of transparent samples, *Nat. Protoc.* 8 (2013) 1535-1550.

- [40] F.S. Rodembusch, L.F. Campo, F.P. Leusin, V. Stefani, Excited state intramolecular proton transfer in amino 2-(2'-hydroxyphenyl)benzazole derivatives. Effects of the solvent and the amino group position, *J. Lumin.* 126 (2007) 728-734.
- [41] P. Ravikumar, G.S.B. Raolji, K.V. Sastry, S. Kalidasu, T. Balaaraju, Design, synthesis, and anticancer evaluation of tetrazole-fused benzoxazole derivatives as tubulin binding agents, *Russ. J. General Chem.* 88 (2018) 2183-2189.
- [42] S. Narva, S. Chitti, S. Amaroju, S. Goud, M. Alvala, D. Bhattacharjee, N. Jain, C.S.K.V. Gowri, Design, synthesis, and biological evaluation of 2-(4-aminophenyl) benzothiazole analogues as antiproliferative agents, *J. Heterocyclic Chem.* 56 (2019) 520-532.
- [43] J.R. Lakowicz, In: *Principles of Fluorescence Spectroscopy*. 3rd ed. New York: Springer; 2006.
- [44] D.P. Heller, C.L. Greenstock, Fluorescence lifetime analysis of DNA intercalated ethidium bromide and quenching by free dye, *Biophys. Chem.* 50 (1994) 305-312.
- [45] J. Borowska, M. Sierant, E. Sochacka, D. Sanna, E. Lodyga-Chruscinska, DNA binding and cleavage studies of copper(II) complexes with 2'-deoxyadenosine modified histidine moiety, *J. Biol. Inorg. Chem.* 20 (2015) 989-1004.
- [46] H. Rozenberg, D. Rabinovich, F. Frolow, R.S. Hegde, Z. Shakked, Structural code for DNA recognition revealed in crystal structures of papillomavirus E2-DNA targets, *Proc. Natl. Acad. Sci. USA* 95 (1998) 15194-15199.
- [47] E.F. Pettersen, T.D. Goddard, C.C Huang, G.S. Couch, D.M. Greenblatt, E.C. Meng, T.E. Ferrin, UCSF Chimera-A visualization system for exploratory research and analysis, *J. Comput. Chem.* 25 (2004) 1605-1162.
- [48] M.D. Hanwell, D.E. Curtis, D.C. Lonie, T. Vandermeersch, E. Zurek, G.R. Hutchison, Avogadro: An advanced semantic chemical editor, visualization, and analysis platform. *J. Cheminform.* 4 (2012) 1-17.
- [49] J.J.P. Stewart, Optimization of parameters for semiempirical methods V: Modification of NDDO approximations and application to 70 elements, *J. Mol. Mod.* 13 (2007) 1173-1213.

- [50] G.M. Morris, R. Huey, W. Lindstrom, M.F. Sanner, R.K. Belew, D.S. Goodsell, A.J. Olson, AutoDock4 and AutoDockTools4: automated docking with selective receptor flexibility, *J. Comput. Chem.* 30 (2009) 2785-2791.
- [51] O. Trott, A.J. Olson, AutoDock Vina: improving the speed and accuracy of docking with a new scoring function, efficient optimization and multithreading, *J. Comput. Chem.* 31 (2010) 455-461.
- [52] Dassault Systèmes BIOVIA, Discovery Studio Modeling Environment, San Diego: Dassault Systèmes, 2016.
- [53] T.H. Dunning, Gaussian basis sets for use in correlated molecular calculations. I. The atoms boron through neon and hydrogen, *J. Chem. Phys.* 90 (1989) 1007-1023.
- [54] E. Papajak, J. Zheng, X. Xu, H.R. Leverentz, D.G. Truhlar, Perspectives on basis sets beautiful: seasonal plantings of diffuse basis functions, *J. Chem. Theory Comput.* 7 (2011) 3027-3034.
- [55] R.L. Martin, Natural transition orbitals, *J. Chem. Phys.* 118 (2003) 4775-4777.
- [56] Gaussian 16, Revision A.03, M.J. Frisch, G.W. Trucks, H.B. Schlegel, G.E. Scuseria, M.A. Robb, J.R. Cheeseman, G. Scalmani, V. Barone, G.A. Petersson, H. Nakatsuji, X. Li, M. Caricato, A.V. Marenich, J. Bloino, B.G. Janesko, R. Gomperts, B. Mennucci, H.P. Hratchian, J.V. Ortiz, A.F. Izmaylov, J.L. Sonnenberg, D. Williams-Young, F. Ding, F. Lipparini, F. Egidi, J. Goings, B. Peng, A. Petrone, T. Henderson, D. Ranasinghe, V.G. Zakrzewski, J. Gao, N. Rega, G. Zheng, W. Liang, M. Hada, M. Ehara, K. Toyota, R. Fukuda, J. Hasegawa, M. Ishida, T. Nakajima, Y. Honda, O. Kitao, H. Nakai, T. Vreven, K. Throssell, J.A. Montgomery Jr., J.E. Peralta, F. Ogliaro, M.J. Bearpark, J.J. Heyd, E.N. Brothers, K.N. Kudin, V.N. Staroverov, T.A. Keith, R. Kobayashi, J. Normand, K. Raghavachari, A.P. Rendell, J.C. Burant, S.S. Iyengar, J. Tomasi, M. Cossi, J.M. Millam, M. Klene, C. Adamo, R. Cammi, J.W. Ochterski, R.L. Martin, K. Morokuma, O. Farkas, J.B. Foresman, D.J. Fox, Gaussian, Inc., Wallingford CT, 2016.
- [57] T.L. Bahers, C. Adamo, I. Ciofini, A qualitative index of spatial extent in charge-transfer excitations, *J. Chem. Theory Comput.*, 7 (2011) 2498-2506.
- [58] T. Lu, Software Multiwfn (<https://www.multiwfn.codeplex.com/>)

- [59] J. Baker, Techniques for geometry optimization: a comparison of cartesian and natural internal coordinates, *J. Comput. Chem.* 14 (1993) 1085-1100.
- [60] G. Ghigo, B.O. Roos, P. Malmqvist, A modified definition of the zeroth-order hamiltonian in multiconfigurational perturbation theory (CASPT2), *Chem. Phys. Lett.* 396 (2004) 142-149.
- [61] N. Forsberg, P. Malmqvist, Multiconfiguration perturbation theory with imaginary level shift, *Chem. Phys. Lett.* 274 (1997) 196-204.
- [62] F. Aquilante, J. Autschbach, R.K. Carlson, L.F. Chibotaru, M.G. Delcey, L. De Vico, I.F. Galván, N. Ferré, L.M. Frutos, L. Gagliardi, M. Garavelli, A. Giussani, C.E. Hoyer, G.L. Manni, H. Lischka, D. Ma, P. Malmqvist, T. Müller, A. Nenov, M. Olivucci, T.B. Pedersen, D. Peng, F. Plasser, B. Pritchard, M. Reiher, I. Rivalta, I. Schapiro, J. Segarra-Martí, M. Stenrup, D.G. Truhlar, L. Ungur, A. Valentini, S. Vancoillie, V. Veryazov, V.P. Vysotskiy, O. Weingart, F. Zapata, R. Lindh, Molcas8: New capabilities for multiconfigurational quantum chemical calculations across the periodic table, *J. Comput. Chem.* 37 (2015) 506-541.
- [63] Iboview software. <http://www.iboview.org/index.html>.
- [64] T. Eicher, S. Hauptam, A. Speicher, *The Chemistry of Heterocycles-Structure, Reactions, Syntheses and Application*, 2nd ed., Wiley-VCH GmbH, 2003.
- [65] R. Vinodkumar, S.D. Vaidya, B.V.S. Kumar, U.N. Bhise, S.B. Bhirud, U.C. Mashelkar, Synthesis, anti-bacterial, anti-asthmatic and anti-diabetic activities of novel N-substituted 2-(4-styrylphenyl)-1h-benzimidazole and N-substituted-3[4-(1H-benzimidazole-2-yl)-phenyl]-acrylic acid tert-butyl ester, *Arkivoc* 14 (2008) 37-49.
- [66] S.J. Strickler, R.A. Berg, Relationship between absorption intensity and fluorescence lifetime of molecules, *J. Chem. Phys.* 37 (1962) 814-822.
- [67] N.J. Turro, J.C. Scaiano, V. Ramamurthy, *Principles of molecular photochemistry: An Introduction*, University Science Book, 1st edn, 2008.
- [68] K. Nishiyama, Y. Watanabe, N. Yoshida, F. Hirata, Solvent dependence of stokes shift for organic solute-solvent systems: a comparative study by spectroscopy and reference interaction-site model-self-consistent-field theory, *J. Chem. Phys.* 139 (2013) 094503.

- [69] J. Soto, J.C. Otero, F.J. Avila, D. Peláez, Conical intersections and intersystem crossings explain product formation in photochemical reactions of aryl azides, *Phys. Chem. Chem. Phys.* 21 (2019) 2389-2396.
- [70] L.J. O'Connor, I.N. Mistry, S.L. Collins, L.K. Folkes, G. Brown, S.J. Conway, E.M. Hammond, CYP450 enzymes effect oxygen-dependent reduction of azide-based fluorogenic dyes, *ACS Central Sci.* 3 (2016) 20-30.
- [71] K. Sivakumar, F. Xie, B.M. Cash, S. Long, H.N. Barnhill, Q. Wang, A Fluorogenic 1,3-dipolar cycloaddition reaction of 3-azidocoumarins and acetylenes, *Org. Lett.* 6 (2004) 4603-4606.
- [72] B. Peng, Z. Gao, X. Li, T. Li, G. Chen, M. Zhou, J. Zhang, DNA binding, DNA cleavage and HSA interaction of several metal complexes containing N-(2-Hydroxyethyl)-N'-benzoylthiourea and 1,10-phenanthroline ligands, *J. Biol. Inorg. Chem.* 21 (2016) 903-916.
- [73] M. Montalti, A. Credi, L. Prodi, M.T. Gandolfi, *Handbook of Photochemistry*, 3rd ed., Taylor & Francis, CRC Press, 2006.
- [74] F. Darabi, H. Hadadzadeh, J. Simpsonb, A. Shahpiric, A water-soluble Pd(II) complex with a terpyridine ligand: experimental and molecular modeling studies of the interaction with DNA and BSA; and in vitro cytotoxicity investigations against five human cancer cell lines. *New J. Chem.* 40 (2016) 9081-9097.
- [75] H.J. Karlsson, M.H. Bergqvist, P. Lincoln, G. Westman, Syntheses and DNA-binding studies of a series of unsymmetrical cyanine dyes: structural influence on the degree of minor groove binding to natural DNA, *Bioorg. Med. Chem.* 12 (2004) 2369-2384.
- [76] C.T. Zeyrek, B. Boyacioglu, O. Temiz-Arpaci, H. Ünver, A. Elmali, Spectroscopic, quantum mechanical and molecular docking studies of a new benzoxazole compound with an oxidoreductase enzyme and DNA, *J. Mol. Struct.* 1136 (2017) 112-126.
- [77] S. Zehra, S. Tabassum, H.A. Al-Lohedan, A. Arjmand, A zwitterionic Zn(II) benzothiazole nanohybrid conjugate as hydrolytic DNA cleavage agent, *Inorg. Chem. Commun.* 93 (2018) 69-72.

[78] F.S. Grasel, T.E. Oliveira, P.A. Netz, Investigation of the interaction of 2-(2'-hydroxyphenyl)-benzoxazoles and their derivatives with B-DNA by docking and molecular dynamics, *J. Braz. Chem. Soc.* 26 (2015) 420-433.

[79] A. Kamal, K.S. Reddy, M.N. Khan, R.V. Shetti, M.J. Ramaiah, S.N. Pushpavalli, C. Srinivas, M. Pal-Bhadra, M. Chourasia, G.N. Sastry, A. Juvekar, S. Zingde, M. Barkume, Synthesis, DNA-binding ability and anticancer activity of benzothiazole/benzoxazole-pyrrolo [2,1-c][1,4]benzodiazepine conjugates, *Bioorg. Med. Chem.* 18 (2010) 4747-4761.

Journal Pre-proof

- Strong interaction with CT-DNA, related to π -stacking and/or intermolecular hydrogen-bonding
- Azido derivatives presented intrinsic fluorescence quenching
- Low-lying excited states and conical intersection of amino and azido benzazole heterocycles by electronic structure methods

Journal Pre-proof

Synthesis, photophysical characterization, CASSCF/CASPT2 calculations and CT-DNA interaction study of amino and azido benzazole analogues

Eduarda S. Gil,^{at} Cláudia B. da Silva,^{at} Pablo A. Nogara,^b Carolina H. da Silveira,^c João B. T. da Rocha,^b Bernardo A. Iglesias,^c Diogo S. Lüdtkke,^a Paulo F. B. Gonçalves,^{*a} Fabiano S. Rodembusch^{*a}

^aInstituto de Química, Universidade Federal do Rio Grande do Sul, UFRGS. Av. Bento Gonçalves 9500, 91501-970, Porto Alegre, RS, Brazil. E-mail: rodembusch@iq.ufrgs.br (Fabiano S. Rodembusch) and paulo@iq.ufrgs.br (Paulo F. B. Gonçalves)

^bLaboratório de Bioquímica Toxicológica, Departamento de Bioquímica e Biologia Molecular, Universidade Federal de Santa Maria, 97105-900, Santa Maria, RS, Brazil.

^cLaboratório de Bioinorgânica e Materiais Porfirínicos, Universidade Federal de Santa Maria, 97105-900, Santa Maria, RS, Brazil.

[†]Both authors contributed equally to this work

Declarations of interest: none